

METHODS FOR SIMULATING AND ANALYZING QUANTUM TURBULENCE OF
BECS IN A ROTATING FRAME

by

Daniel Kyle Foshee

Copyright © Daniel Kyle Foshee 2023

A Thesis Submitted to the Faculty of the

JAMES C. WYANT COLLEGE OF OPTICAL SCIENCES

In Partial Fulfillment of the Requirements

For the Degree of

MASTER OF SCIENCE

In the Graduate College

THE UNIVERSITY OF ARIZONA

2023

THE UNIVERSITY OF ARIZONA
GRADUATE COLLEGE

As members of the Master’s Committee, we certify that we have read the thesis prepared by **Daniel Foshee**, titled *Methods for Simulating and Analyzing Quantum Turbulence of BECs in a Rotating Frame* and recommend that it be accepted as fulfilling the thesis requirement for the Master’s Degree.



Professor Brian P. Anderson

Date: 7/25/23



Professor Ewan M. Wright

Date: 7/25/23

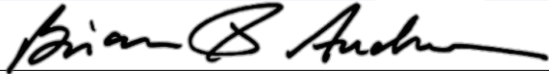


Professor Ashton Bradley

Date: 8/01/23

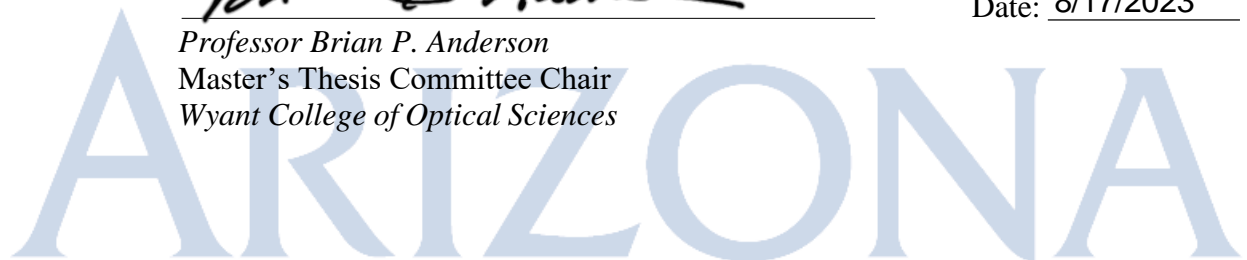
Final approval and acceptance of this thesis is contingent upon the candidate’s submission of the final copies of the thesis to the Graduate College.

I hereby certify that I have read this thesis prepared under my direction and recommend that it be accepted as fulfilling the Master’s requirement.



Professor Brian P. Anderson
Master’s Thesis Committee Chair
Wyant College of Optical Sciences

Date: 8/17/2023



Acknowledgements

I would like to start by giving my deepest gratitude to my advisor, Brian Anderson, who taught me everything I know about quantum mechanics. To him I owe a debt that I could never repay with his consistent and gratuitous generosity. He gave the time, patience, guidance, and expertise that made this entire project possible. Next, I'd like to thank the members of my committee Ashton Bradley whose wealth of knowledge was invaluable for creating a working project that avoided several major pitfalls and Ewan Wright who assured the accuracy and quality of my work. I'd also like to acknowledge the time and advice given to me by Matt Reeves, Tyler Neely, and Matthew Davis towards the end of the project which helped me aim the final sections of my research. I'd also like to thank the students who worked with me during my time at the University of Arizona. This is especially true of Jennifer Bragg who helped keep me sane while working through the online program. All of this would be impossible without my parents who always supported me. You gave me access to all the opportunities that I needed to get here. There is a huge community of people who have helped me develop to who I am today. I have been lucky to have many great role models, coaches, teachers, and friends. Finally, I'd like to thank Troy Glatfelter, Barbara Grant, and Keith Kasunic who advocated for my success and the UA staff that put in a huge amount of effort and care to make the online program possible.

Land Acknowledgment

We respectfully acknowledge the University of Arizona is on the land and territories of Indigenous peoples. Today, Arizona is home to 22 federally recognized tribes, with Tucson being home to the O'odham and the Yaqui. Committed to diversity and inclusion, the University strives to build sustainable relationships with sovereign Native Nations and Indigenous communities through education offerings, partnerships, and community service.

Table of Contents

List of Figures	9
List of Tables.....	11
Abstract.....	13
Chapter 1. Introduction and Motivation.....	14
1.1 Brief Literature Review and Motivation.....	15
Chapter 2. Physics Review and Simulation Building	19
2.1 Time Evolution in Quantum Mechanics	19
2.2 The Hamiltonian	20
2.3 The Magnetic Trap.....	20
2.4 The Laser.....	21
2.5 Stirring with the Laser.....	22
2.6 Calculation of Laser Power	22
2.7 Interaction Energy.....	24
2.8 Calculation of the Interaction Coefficient in 2D	25
2.9 Split-Step Calculation of the Time Evolution	26
2.10 Damping to the Ground State	26
2.11 Damping to a Rotating Frame via Gross–Pitaevskii Equation and Split-Step Time Evolution	27

2.12 Rotational Split-Step Algorithm	27
2.13 Running a Simulation.....	29
Chapter 3. Data	30
3.1 Set 1 – Experiment 1 – Low Damping Baseline	40
3.2 Set 1 – Experiment 2 – Smaller Laser.....	41
3.3 Set 1 – Experiment 3 – Bigger Laser	42
3.4 Set 1 – Experiment 4 – Smaller Frequency.....	43
3.5 Set 1 – Experiment 5 – Larger Frequency.....	44
3.6 Set 2 – Experiment 1 – No Laser.....	45
3.7 Set 2 – Experiment 2 – Faster Frequency	46
3.8 Set 2 – Experiment 3 – Less Eccentric Trap	47
3.9 Set 2 – Experiment 4 – Dimpled Condensate.....	48
3.10 Set 3 – Experiment 1 – Larger Dimple	49
3.11 Set 3 – Experiment 2 – Dimpled, Round Trap and Laser	50
3.12 Set 3 – Experiment 3 – Dimpled, Round Trap	51
3.13 Set 3 – Experiment 4 – Dimpled, Round Laser	52
3.14 Set 4 – Experiment 1 – Dimpled with Lower Eccentricity	53
3.15 Set 4 – Experiment 2 – Dimpled with Alternate Rotation	54
3.16 Set 4 – Experiment 3 – Dimpled, Alternate Laser Rotation.....	55

3.17 Set 4 – Experiment 4 – Dimpled, Alternate Trap Rotation.....	56
3.18 Set 5 – Experiment 1 – No Damping.....	57
3.19 Set 5 – Experiment 2 – Rotating Frame and Stirring Slowed.....	58
3.20 Set 5 – Experiment 3 – Rotating Frame Slowed.....	59
3.21 Set 11 – Experiment 1 – 6 Still Gaussian Lasers.....	60
3.22 Set 11 – Experiment 2 – 6 Rotating Gaussian Lasers.....	61
3.23 Set 11 – Experiment 3 – Much Less Laser Power, Reversed.....	62
3.24 Set 11 – Experiment 4 –Less Laser Power, Reversed.....	63
3.25 Set 12 – Experiment 1 –Speckled Annulus.....	64
3.26 Missing Sets 6-10.....	65
3.26.1 Set 6 – Much Larger Dimples.....	65
3.26.2 Set 7 – Stronger Damping and Different Stirring Rates.....	65
3.26.3 Set 8 – Computation Timing.....	65
3.26.4 Set 9 – Laser Convolution.....	66
3.26.5 Set 10 – Polygonal Boundaries.....	66
Chapter 4. Analytical Methods.....	67
4.1 Method 1 – Observing Density Over Time.....	67
4.2 Method 2 – Observing Vorticity Over Time.....	68
4.2.1 Vorticity Analysis Applied to our Data.....	69

4.3 Method 3 – Moving Averages	71
4.4 Method 4 – Speed Maps with Streamlines.....	72
4.5 Methods not Implemented.....	74
4.5.1 Tracer Particles	74
4.5.2 Energy Spectrum Plots	74
Chapter 5. Conclusion.....	75
Appendix A: Moving MATLAB Calculations to the Graphical Processing Unit	77
Appendix B: Moving Calculations to The University of Arizona High-Powered Computing Cluster	79
B.1 Starting MATLAB on The University of Arizona’s HPC Cluster.....	79
B.2 Downloading/Uploading from/to the HPC.....	83
B.3 Final note on the HPC	83
Appendix C: Using Our Code	83
C.1 General Algorithm.....	83
C.2 Stages.....	84
C.3 Stages File.....	85
C.4 Settings File	85
C.5 Contents of the Settings File	86
References	90

List of Figures

Figure 1.1	North polar region of Jupiter	15
Figure 1.2	North polar region of Saturn	16
Figure 1.3	Saturn-like vortex structure in liquid water	17
Figure 3.1	Density analysis of set 1, experiment 1	40
Figure 3.2	Density analysis of set 1, experiment 2	41
Figure 3.3	Density analysis of set 1, experiment 3	42
Figure 3.4	Density analysis of set 1, experiment 4	43
Figure 3.5	Density analysis of set 1, experiment 5	44
Figure 3.6	Density analysis of set 2, experiment 1	45
Figure 3.7	Density analysis of set 2, experiment 2	46
Figure 3.8	Density analysis of set 2, experiment 3	47
Figure 3.9	Density analysis of set 2, experiment 4	48
Figure 3.10	Density analysis of set 3, experiment 1	49
Figure 3.11	Density analysis of set 3, experiment 2	50
Figure 3.12	Density analysis of set 3, experiment 3	51
Figure 3.13	Density analysis of set 3, experiment 4	52
Figure 3.14	Density analysis of set 4, experiment 1	53
Figure 3.15	Density analysis of set 4, experiment 2	54
Figure 3.16	Density analysis of set 4, experiment 3	55
Figure 3.17	Density analysis of set 4, experiment 4	56
Figure 3.18	Density analysis of set 5, experiment 1	57
Figure 3.19	Density analysis of set 5, experiment 2	58
Figure 3.20	Density analysis of set 5, experiment 3	59
Figure 3.21	Density analysis of set 11, experiment 1	60
Figure 3.22	Density analysis of set 11, experiment 2	61

Figure 3.23	Density analysis of set 11, experiment 3	62
Figure 3.24	Density analysis of set 11, experiment 4	63
Figure 3.25	Density analysis of set 12, experiment 1	64
Figure 4.1	Density analysis of set 1, experiment 1	68
Figure 4.2	Vorticity analysis proof of concept	69
Figure 4.3	Vorticity analysis applied to our data	70
Figure 4.4	Moving average of density analysis of set 12, experiment 1	71
Figure 4.5	Speed map of set 12, experiment 1 overlaid with streamlines	73
Figure C.1	Online interface for starting MATLAB on the UA HPC	80
Figure C.2	Settings interface for the UA HPC computation	81
Figure C.3	The queuing interface for starting a computation on the UA HPC	82
Figure C.4	The launching GUI for MATLAB on the UA HPC	82

List of Tables

Table 3.1	Constants used in the simulation	31
Table 3.2	Symbol definitions and their units	32
Table 3.3	Parameters for the first set of experiments	33
Table 3.4	Parameters for the second set of experiments	34
Table 3.5	Parameters for the third set of experiments	35
Table 3.6	Parameters for the fourth set of experiments	36
Table 3.7	Parameters for the fifth set of experiments	37
Table 3.8	Parameters for the sixth set of experiments, MATLAB set 11	38
Table 3.9	Parameters for the seventh set of experiments, MATLAB set 12	39
Table 3.10	A shortened version of Table 3.3 for set 1, experiment 1	40
Table 3.11	A shortened version of Table 3.3 for set 1, experiment 2	41
Table 3.12	A shortened version of Table 3.3 for set 1, experiment 3	42
Table 3.13	A shortened version of Table 3.3 for set 1, experiment 4	43
Table 3.14	A shortened version of Table 3.3 for set 1, experiment 4	44
Table 3.15	A shortened version of Table 3.4 for set 2, experiment 1	45
Table 3.16	A shortened version of Table 3.4 for set 2, experiment 2	46
Table 3.17	A shortened version of Table 3.4 for set 2, experiment 3	47
Table 3.18	A shortened version of Table 3.4 for set 2, experiment 4	48
Table 3.19	A shortened version of Table 3.5 for set 3, experiment 1	49
Table 3.20	A shortened version of Table 3.5 for set 3, experiment 2	50
Table 3.21	A shortened version of Table 3.5 for set 3, experiment 3	51
Table 3.22	A shortened version of Table 3.5 for set 3, experiment 4	52
Table 3.23	A shortened version of Table 3.6 for set 4, experiment 1	53
Table 3.24	A shortened version of Table 3.6 for set 4, experiment 2	54
Table 3.25	A shortened version of Table 3.6 for set 4, experiment 3	55

Table 3.26	A shortened version of Table 3.6 for set 4, experiment 4	56
Table 3.27	A shortened version of Table 3.7 for set 5, experiment 1	57
Table 3.28	A shortened version of Table 3.7 for set 5, experiment 2	58
Table 3.29	A shortened version of Table 3.7 for set 5, experiment 3	59
Table 3.30	A shortened version of Table 3.7 for set 11, experiment 1	60
Table 3.31	A shortened version of Table 3.8 for set 11, experiment 2	61
Table 3.32	A shortened version of Table 3.8 for set 11, experiment 3	62
Table 3.33	A shortened version of Table 3.8 for set 11, experiment 4	63
Table 3.34	A shortened version of Table 3.9 for set 12, experiment 1	64

Abstract

The relationships between turbulence and interesting fluid structures like those near the poles of Jupiter and Saturn are still an open research topic. A minimal model for understanding fundamental behaviors is desirable for isolating the relevant parameter space with predictive power. Minimal models in liquids inspire us to look for a more minimal model in 2D Bose-Einstein Condensates. We have created a framework for quickly simulating and analyzing 2D Bose-Einstein Condensates in a rotating reference frame to test a wide range of parameter space via the MATLAB parallel computing toolbox, the utilization of a graphics processing unit, and the high-powered computing cluster available to us through the University of Arizona. In the development of these methods, we find that our novel application of qualitative analysis shows evidence that differential rotation leads to the observation of counter-rotating eddies consistent with the development of characteristic structures from turbulent fluid flow. This work sets up a platform for researching quantum turbulence in 2D Bose-Einstein condensates evolving under differential rotation in a rotating frame and gives direction for research that may have connection to classical phenomena seen in the atmospheres of the gas giants of our solar system and in liquid models here on Earth.

Chapter 1. Introduction and Motivation

Quantum mechanics has led to some of the most accurate and confounding predictions in modern physics, and where those confusing and surprising phenomena are found it is often helpful to have visual confirmation. This is the world of Bose-Einstein condensate (BEC) physics. BEC Physics studies macroscopic quantum behavior that is visibly observable [1]. In our thesis, we take motivation from classical atmospheric dynamics in two gas giant planets of our solar system and look for similarities or differences in a quantum fluid.

In this thesis, we first look at classical fluids in the atmospheres of Saturn and Jupiter [2], and in laboratories on Earth [3]. Inspired to create a more minimal model, we set up a framework for simulating and analyzing fluid flow properties in a two-dimensional (2D) BEC in a rotating reference frame. In this 2D BEC in a rotating frame, we simulate perturbing the condensate with time-varying magnetic and optical potentials. In the creation of this framework, we find evidence suggesting that the methods of perturbation explored here may be an effective way to create predictably turbulent flow patterns in 2D BECs in a rotating frame that have some similarities to the atmospheric dynamics of gas giants.

There are nevertheless certain interesting and unique aspects of studying quantum turbulence of a 2D BEC in a rotating frame. BEC behavior is described well by mean-field theory [1] being representative of real experimental situations for corresponding parameters, and reducing to the 2D approximation makes the calculation and analysis simpler. Further, being in a rotating frame has the potential for polarizing all vortices in the condensate. There are two main implications of this. The first is that without uncertainty of polarity of the vortices, visual observation of the condensate would give position and polarity of all vortices in typical experimental observations [4]. In the limit that turbulent energy is dominated by incompressible energy (i.e., vortices rather than sound waves), it also implies approximate analytical knowledge of the quantum phase profile and thus the fluid flow profile of the entire condensate [5]. Moreover, when all vortices have the same polarity, conversion of incompressible energy to compressible energy via vortex annihilation is suppressed. Altogether, these aspects allow for

attempting to match analytical quantum fluid dynamics with observed behaviors and make accurate predictions and explanations. With these considerations in mind, we have created a framework for simulating and analyzing 2D BEC quantum fluid dynamics in a rotating frame, and we hope that it will help future researchers understand certain aspects of quantum turbulence better.

1.1 Brief Literature Review and Motivation

From storms bigger than planets to small buckets here on Earth, turbulence is a universal phenomenon [6]. We look to push the boundaries of BEC physics with inspiration from some of the most interesting fluid dynamics in our solar system, and in doing so, probe aspects of turbulence universality [6]. Chief among these are the vortex systems in the polar regions of Jupiter and Saturn.

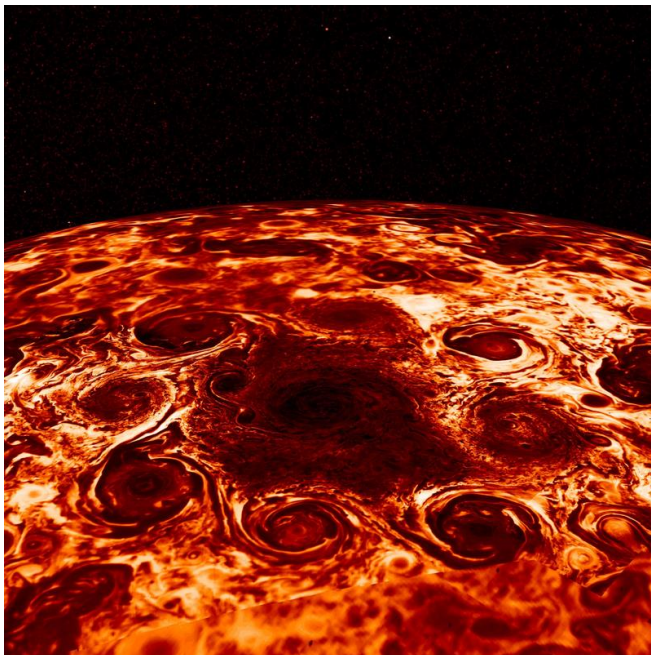


Figure 1.1: Vortex Structure at Jupiter's North Pole captured by NASA's Juno spacecraft [7].

Credits: NASA/JPL-Caltech/SwRI/ASI/INAF/JIRAM

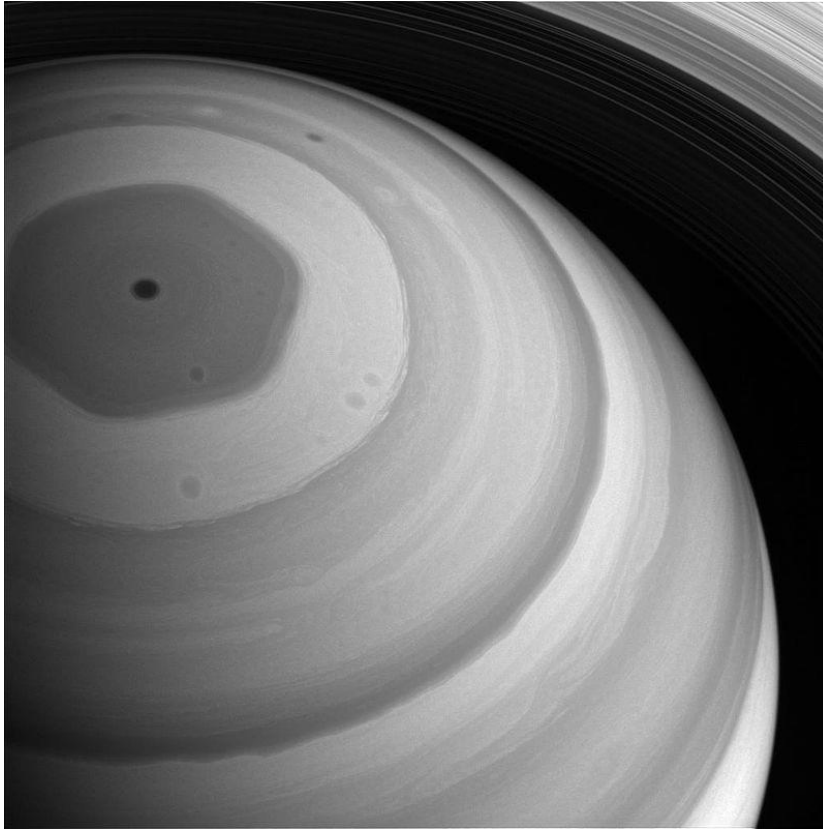


Figure 1.2: Hexagon at Saturn's North Pole captured by Cassini [8]. Credits: NASA/JPL-Caltech/Space Science Institute.

On the north pole of Jupiter, a characteristic structure of atmospheric long-lived vortices is observed, and on the north pole of Saturn a long-lived characteristic hexagon structure is observed [2]. The characteristic structures of these turbulent systems, observed in Jupiter and Saturn, have piqued the curiosity of scientists since their respective discoveries. Our hypothesis is that similar behaviors may be seen in BECs under differential rotation, as exists in these planetary atmospheres [2]. Assuming the entire planet is rotating at the same rotational frequency, different latitudes having different tangential velocities may lead to shearing in the fluid. Shearing in fluids causes turbulent fluid flow that may be partially responsible for these characteristic structures.

Although both quasi-2D and 3D explanations have been proposed for the behavior observed in these planetary systems [2], we find this paper, *A Laboratory Model of Saturn's North Polar Hexagon* [3], makes a compelling case that this type of behavior can be seen in quasi-2D systems for which velocity gradients in one spatial dimension are negligible compared to overall velocity gradients. In this paper [3], vortex structures like that on Saturn are found by creating differential rotation in a liquid fluid in a rotating bucket. On the surface of the liquid, shallow contact is made at a second rotational frequency that is slightly higher than that of the bucket.

The main parameters explored were the relative rotational rates and the viscosity of the liquid. In the exploration of that parameter space, the authors found that combinations of parameters could predict steady modal behavior like that shown in Figure 1.3, which is comparable to the northern polar region of Saturn [3].

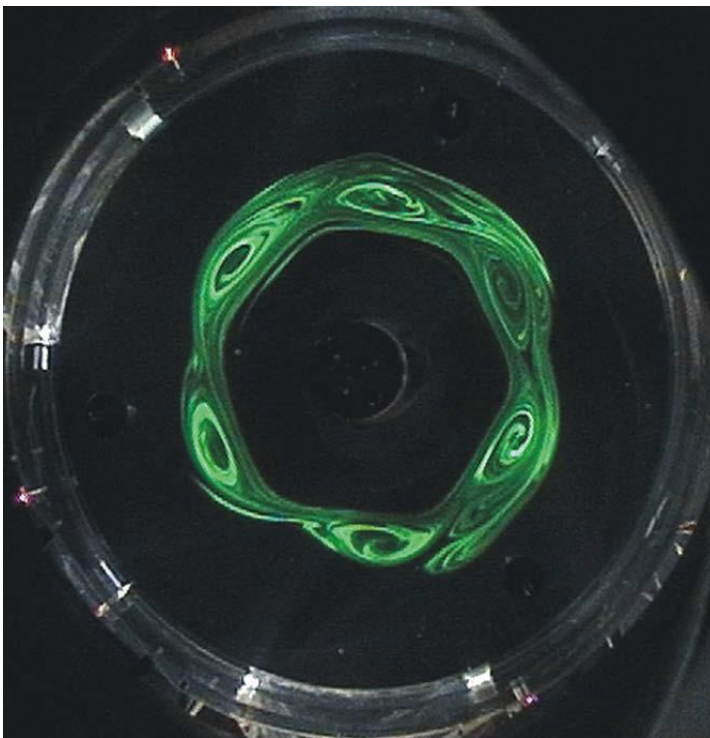


Figure 1.3: Saturn-like vortex structure in a rotating bucket of water and glycerin under differential rotation – *A Laboratory Model of Saturn's North Polar Hexagon*, Figure 10 [3].

In *A Laboratory Model of Saturn's North Polar Hexagon*, the authors argue that the formation of the characteristic structures is due to differential rotation that gives rise to instabilities [3]. We wish to examine the dynamics of BECs forced by a system of optical and magnetic potentials to evolve under differential rotation and velocity gradients.

We have two main goals for this research. The first is to set up a numerical model of a 2D BEC in a rotating frame that would be easily adaptable to studying the dynamics of BECs evolving under differential rotation for realistic experimental conditions. Our second main goal is to begin to explore the enormous dynamical phase space of BECs under differential rotation in order to identify new unique features and parameter spaces for future research of these systems.

For most of our simulations, we start by damping the BEC into the ground state of a rotating frame, forming a vortex lattice. Then, we attempt to create differential rotation by stirring radially across the condensate with simulated optical potentials.

The rest of this thesis is laid out in the following way. In Chapter 2, we review physical phenomena involved in our simulated experiments and describe the mathematical and algorithmic framework for setting up our simulations. In Chapter 3, we discuss the parameters and data found in our simulations. In Chapter 4, we describe the analytical methods attempted and their results. In Chapter 5, we give a conclusion of our study focused on the interesting directions in parameter space for future research. Finally, we have appendices on the topics of parallel computing in MATLAB, using the high-performance computing cluster for University of Arizona affiliates, and using our MATLAB code.

Chapter 2. Physics Review and Simulation Building

The goal of our simulations is to numerically create a 2D BEC in a rotating frame and observe the resultant behavior of different magnetic and optical perturbations that are intended to create differential rotation. The system can be evolved over time using a split-step Fourier transform approach [9]. With an initial wavefunction $\varphi(t)$, a small timestep Δt evolves the wavefunction $\varphi(t)$ to $\varphi(t + \Delta t)$, with the evolution depending on the Hamiltonian for the system. This method is applied repetitiously until arriving at the desired end time. The energies in the system calculated in the Hamiltonian can be sorted into the kinetic energy, the potential energies, and the interaction energy. The potential energies are provided by a magnetic trap and a laser, described in more detail later, and the interaction energy which arises from the mutual repulsion of particles, assumed to be Rubidium-87. Where the condensate has higher density, the aggregated strength of the repulsive interactions will be much higher than where the condensate has lower density. Thus, the interaction term and consequently the entire Hamiltonian is dependent on the time-evolving wavefunction. In calculation, this becomes a non-linear recursive process, the Hamiltonian being dependent on the wavefunction it acts upon. Therefore, the time evolution will take small steps, from one wavefunction in time to the next in time, in the limit that the wavefunction and the Hamiltonian calculated with it does not change much in those steps. The final big picture summary is that in order to observe what happens as the condensate is perturbed, we must slowly evolve the condensate one small step at a time.

2.1 Time Evolution in Quantum Mechanics

The Schrödinger Equation,

$$H|\varphi(t)\rangle = i\hbar \frac{\partial}{\partial t} |\varphi(t)\rangle, \quad (2.1.1)$$

describes the relationship between the change in the state over time and the energies involved in the system, where H is the Hamiltonian, \hbar is Planck's reduced constant, t is time, and $|\varphi(t)\rangle$ is the quantum mechanical state of the system (for us, the BEC) at time t .

We've already noted that the Hamiltonian will be dependent on the density of the condensate. This density will change over time in our simulations looking at fluid flow. Thus, the Hamiltonian will be dependent on time. However, when taking very small steps in time, we can approximately treat the Hamiltonian as independent of time during a small time-step of duration Δt . In this limit, given an initial state at time t , a following state at a later time can be solved via:

$$|\varphi(t + \Delta t)\rangle = e^{-iH\Delta t/\hbar}|\varphi(t)\rangle. \quad (2.1.2)$$

This is the main calculation to be solved in the simulation. The time step must be small enough for approximations to hold. For our simulations, we used a time-step of about 400 nanoseconds.

2.2 The Hamiltonian

As stated previously, the Hamiltonian is comprised of the kinetic energy, the potential energies of the magnetic trap and the laser, and the interaction energy of the particles. The following subsections contain brief descriptions of the potential and interaction energies as they apply to our system and real BEC experiments.

2.3 The Magnetic Trap

Magnetic fields are commonly used to trap and manipulate BECs. For our simulations, we explored the use of a harmonic oscillator potential shown here:

$$V = \frac{1}{2}m\omega_x^2x^2 + \frac{1}{2}m\omega_y^2y^2 + \frac{1}{2}m\omega_z^2z^2, \quad (2.3.1)$$

where V is the harmonic oscillator potential, m is the atomic mass, and ω_x , ω_y , and ω_z are the trap frequencies in the x -direction, y -direction, and z -direction respectively.

The BEC is trapped in 3 dimensions, but the frequency of the parabolic trap is much higher in one direction than the other two. In this configuration, the BEC can take on a highly oblate, round shape like a pancake. We will refer to the dimension of the trap with a large trap frequency the z -direction and the other dimensions as the x -direction and y -direction.

The x -direction and y -direction trap frequencies can be made equal, giving a perfectly round BEC, or they can be adjusted in frequency with one becoming slightly higher than the other. We will describe this squeezing as an eccentricity. This eccentricity can be applied at different angles at some angular frequency to create a stirring effect on the condensate from the rotation of the eccentricity of the trap as was first explored to create vortices in [10]. In shorthand, we will refer to this as “rotation of the eccentric trap.” For the purposes of our study, eccentricity is defined in the following way:

$$\varepsilon = \frac{\omega_y - \omega_x}{\bar{\omega}} \quad (2.3.2)$$

$$\omega_x = \bar{\omega}(1 - \varepsilon) \quad (2.3.3)$$

$$\omega_y = \bar{\omega}(1 + \varepsilon) \quad (2.3.4)$$

$$\bar{\omega} = \frac{\omega_x + \omega_y}{2} \quad (2.3.5)$$

where ε is the eccentricity, and $\bar{\omega}$ is the average trap frequency.

2.4 The Laser

In order to create other potential energy landscapes or stir the condensate, a blue-detuned laser with a frequency much higher than the resonant frequency of the ^{87}Rb atoms were

simulated. This far blue-detuned laser can push particles of the ^{87}Rb condensate away from the laser due to the optical dipole potential,

$$V_{dipole} = \frac{\hbar\Gamma}{8} \frac{I_{\max} / I_{\text{sat}}}{\Delta / \Gamma}, \quad (2.4.1)$$

where Γ is the decay rate of atomic transition that is perturbed by the laser, and Δ is the detuning from this resonant frequency. I_{\max} is the maximum intensity of the laser, and I_{sat} is the saturation intensity for this atomic transition.

2.5 Stirring with the Laser

One method of stirring the condensate would be to make a stir bar analogue in the condensate with the laser. A simple version would be to have a gaussian with one cardinal dimension wider than the other. This shape would then be rotated in the condensate over time at some angular frequency. This method has been explored as one way to cause fluid flow in the condensate. We will refer to it as “rotation of the eccentric laser.” In a stationary frame, this method has also been explored to nucleate vortices [11] [12].

There are endless other ways to design laser potentials, but one in which we are interested is a rotating annulus. We attempted one annulus with a series of identical gaussians that rotate and another with a superposition of random width and height gaussians.

2.6 Calculation of Laser Power

An important parameter to staging this experiment is an understanding of the laser power involved to see the desired effect. Although there is a relationship between intensity and potential energy of the atoms, lasers are more often specified in laser power rather than intensity.

Thus, if a relationship between total power and maximum intensity is known, for example in a gaussian, this can be used to find relevant laser powers for specific experiments.

Another way to look at laser power is from the maximum potential energy provided by the laser. It may be valuable from an analytical perspective to know what its relationship is to the characteristic energy of the BEC, the chemical potential [1].

For all of these reasons, the following algorithm is used to find the laser power which is then converted into an intensity to find the potential energy added to the system.

- 1) In the Thomas-Fermi approximation [1], the chemical potential can be expressed in terms of $\bar{\omega}$, the geometric mean of the trap frequencies; N , the number of atoms; a_{scat} , the s -wave interatomic scattering length; $\bar{\sigma}$, the geometric mean of the characteristic harmonic oscillator lengths; and m , the atomic mass [13]:

$$\bar{\sigma} = \sqrt{\frac{\hbar}{m\bar{\omega}}}, \quad (2.6.1)$$

$$\mu = \frac{\hbar\bar{\omega}}{2} \left(\frac{15Na_{\text{scat}}}{\bar{\sigma}} \right). \quad (2.6.2)$$

- 2) The maximum potential energy provided by the laser, E_l , can be defined in terms of the chemical potential, μ , and a scalar, f :

$$E_l = \mu * f. \quad (2.6.3)$$

- 3) For a round Gaussian laser beam with $\frac{1}{e^2}$ radius ω_{gauss} , the maximum intensity, I_{max} , of the laser is defined in terms of the total power P_l :

$$I_{\text{max}} = \frac{2P_l}{\pi\omega_{\text{gauss}}^2}. \quad (2.6.4)$$

- 4) Starting from the optical dipole potential, the power of the laser is determined using substitution:

$$E_l = \frac{\hbar\Gamma I_{\max} / I_{\text{sat}}}{8 \Delta / \Gamma}, \quad (2.6.5)$$

$$P_l = \frac{4\pi * E_l * I_{\max} * \Delta * \omega_{\text{gauss}}^2}{\hbar\Gamma^2}. \quad (2.6.6)$$

2.7 Interaction Energy

The 3D Gross-Pitaevskii equation (GPE) is an excellent approximate evolution equation for BEC many-body wavefunction dynamics for scalar wavefunctions of the type considered in our study [1]. It approximates the aggregated effect of many particles interacting, repelling each other in the case of ^{87}Rb , as a density-dependent pseudo-potential energy. This is shown below [1]:

$$(KE + PE + Ng|\varphi(\vec{r}, t)|^2)\varphi(\vec{r}, t) = i\hbar \frac{\partial}{\partial t} \varphi(\vec{r}, t), \quad (2.7.1)$$

where KE is the kinetic energy operator, PE is the potential energy operator, and $Ng|\varphi(\vec{r}, t)|^2$ is the particle interaction term, where $\varphi(\vec{r}, t)$ is the volumetric wavefunction normalized such that the modulus squared of the wavefunction, integrated over the entire volume, is equal to 1,

$$\int |\varphi(\vec{r}, t)|^2 d\vec{r} = 1, \quad (2.7.2)$$

and g is the interaction coefficient defined in terms of the s -wave scattering length mentioned earlier, a_{scat} , and the atomic mass m ,

$$g = \frac{4\pi\hbar^2 a_{\text{scat}}}{m}. \quad (2.7.3)$$

As stated earlier, we will need a starting wavefunction to begin time evolution, so an initial approximation of our wavefunction will need to be calculated. We start with the Thomas-Fermi solution to the ground state of a non-rotating harmonic potential [1]. This approximation assumes that a very large number of particles in the gas causes a large increase in the potential and interaction energy terms. In this limit and in a harmonic magnetic trap, the kinetic energy can be neglected, and the result is the density profile of a downward facing parabola. This will be the starting point for all of our simulations. The ground state wavefunction, density profile, and interaction coefficient are shown below:

$$\varphi(\vec{r}) = \begin{cases} \sqrt{\frac{\mu - V(\vec{r})}{Ng}}, & \text{for } \mu \geq V \\ 0, & \text{for } \mu < V \end{cases} \quad (2.7.4)$$

$$n(\vec{r}) = N|\varphi|^2 \quad (2.7.5)$$

where n is the density profile, N is the number of atoms, V is the potential energy of the magnetic trap, and $\varphi(\vec{r})$ is the normalized many-body wavefunction (for the non-rotating ground state).

2.8 Calculation of the Interaction Coefficient in 2D

For highly oblate harmonic potentials, the 3D GPE can be approximated using a 2D GPE [1]. We approach this approximation using the following relationships:

$$R_z = \sqrt{\frac{2\mu}{m\omega_z}} \quad (2.8.1)$$

$$\sigma_{\text{eff}} = \frac{16R_z}{15\sqrt{\pi}} \quad (2.8.2)$$

$$g_{2D} = \frac{g}{\sigma_{\text{eff}} * \sqrt{2\pi}} \quad (2.8.3)$$

where R_z is the Thomas-Fermi radius in the z -direction, σ_{eff} is the effective characteristic length of the trap in the z -direction, g is the interaction coefficient, and g_{2D} is the approximate 2D interaction coefficient.

2.9 Split-Step Calculation of the Time Evolution

Because some operators within the Hamiltonian do not commute with each other, staying in the same representation for the entire calculation typically requires taking derivatives which are time and calculation intensive. For these reasons, it is typical to do a split-step calculation of the time evolution like the “split-step Fourier Transform method” [9]. With this method half of the potential energy is applied with the wavefunction in the position representation. Next, a Fourier transform of the wavefunction is taken and the kinetic energy is applied in the momentum representation where that calculation is easier. Finally, an inverse Fourier transform is taken, and the second half of the potential energy is applied. This greatly reduces calculation time while still meeting accuracy requirements. We describe our split-step Fourier transform algorithm with relevant equations in Chapter 2, section 12.

2.10 Damping to the Ground State

In the exponential of the time-step evolution, a small additional damping constant, $\gamma \approx 10^{-4}$, is added [5]. This added constant implements exponential decay to the system and causes the system to decay to the state with lowest energy possible, or ground state. This is in the time-step evolution as

$$|\varphi(t + \Delta t)\rangle = e^{-(i+\gamma)H\Delta t/\hbar(1+\gamma^2)}|\varphi(t)\rangle \quad (2.10.1)$$

$$(1 + \gamma^2) \approx 1. \quad (2.10.2)$$

2.11 Damping to a Rotating Frame via Gross–Pitaevskii Equation and Split-Step Time Evolution

To implement a rotating frame, angular momentum terms can be added to the Hamiltonian of our system as the cross-product between the position and momentum operators with higher velocities further from the center of rotation having higher angular momentum. When the system is damped with this angular momentum term in the Hamiltonian, the system's lowest energy state will be a rotating BEC, a vortex lattice [1]. Although this H , shown below, is not a linear Hamiltonian strictly speaking, it is our conceptual description of the energy of the system at any time step used in the evolution for our simulations:

$$H = \frac{1}{2m} (\hat{P}_x^2 + \hat{P}_y^2) + (-\Omega \hat{X} \hat{P}_y + \Omega \hat{Y} \hat{P}_x) + (PE(\hat{X}, \hat{Y}) + IE(\hat{X}, \hat{Y})), \quad (2.11.1)$$

where \hat{P}_x and \hat{P}_y are the momentum operators in the x -direction and y -direction; \hat{X} and \hat{Y} are the position operators; PE represents the total potential energy of the system which is a sum of potential energy contributions from the magnetic trap and the laser; IE represents the energy contributed to the system from particle interactions; and Ω is the rotational frequency which, when non-zero, implements the rotating frame to our approximate description of the energy of the system.

2.12 Rotational Split-Step Algorithm

With our wavefunction beginning in the position representation, we follow these steps to calculate the time-step evolution.

- 1) Apply half of potential energy, PE , and interaction energy, IE :

$$|\varphi_{\text{step1}}\rangle = e^{-(i+\gamma)\left(\frac{1}{2}\right)(PE+IE)\Delta t/\hbar(1+\gamma^2)}|\varphi_{\text{initial}}(t)\rangle. \quad (2.12.1)$$

- 2) Take the 1-D Fourier transform of the wavefunction in the x -direction, shown below:

$$\varphi_{\text{step2}}(p_x, y, t) = FT_x[\varphi_{\text{step1}}(x, y, t)]. \quad (2.12.2)$$

- 3) Apply part of the rotational and kinetic energy terms together, shown below:

$$|\varphi_{\text{step3}}(t)\rangle = e^{-(i+\gamma)\left(\frac{1}{2m}\hat{p}_x^2 + \Omega\hat{Y}\hat{p}_x\right)\Delta t/\hbar(1+\gamma^2)}|\varphi_{\text{step2}}(t)\rangle. \quad (2.12.3)$$

- 4) Take the 1-D inverse Fourier transform of the wavefunction in the x -direction, shown below:

$$\varphi_{\text{step4}}(x, y, t) = FT_x^{-1}[\varphi_{\text{step3}}(p_x, y, t)]. \quad (2.12.4)$$

- 5) Take the 1-D Fourier transform of the wavefunction in the y -direction, shown below:

$$\varphi_{\text{step5}}(x, p_y, t) = FT_y[\varphi_{\text{step4}}(x, y, t)]. \quad (2.12.5)$$

- 6) Apply the other part of the rotational and kinetic energy terms together, shown below:

$$|\varphi_{\text{step6}}(t)\rangle = e^{-(i+\gamma)\left(\frac{1}{2m}\hat{p}_y^2 - \Omega\hat{Y}\hat{p}_y\right)\Delta t/\hbar(1+\gamma^2)}|\varphi_{\text{step5}}(t)\rangle. \quad (2.12.6)$$

- 7) Take the 1-D inverse Fourier transform of the wavefunction in the y -direction, shown below:

$$\varphi_{\text{step7}}(x, y, t) = FT_y^{-1}[\varphi_{\text{step6}}(x, p_y, t)]. \quad (2.12.7)$$

- 8) Apply the second half of the potential energy and interaction energy, shown below:

$$|\varphi_{\text{step8}}(t)\rangle = e^{-(i+\gamma)\left(\frac{1}{2}\right)(PE+IE)\Delta t/\hbar(1+\gamma^2)}|\varphi_{\text{step7}}(t)\rangle. \quad (2.12.8)$$

- 9) Renormalize the wavefunction.

2.13 Running a Simulation

These are the steps for running a general simulation.

- 1) Start with a Thomas-Fermi stationary ground state approximation.
- 2) Evolve time until a (rotating) ground state is found.
- 3) Turn on laser and move magnetic and optical potentials.

Chapter 3. Data

This chapter describes the simulated experiments with their motivations and relevant parameters. Before describing the simulations individually, we describe the group of experiments generally. As we will do for individual cases, we will start with a general description of the experiments. After the general description, we assign symbols for constants and units for the relevant parameters and present a table for the associated values of those parameters for each experiment presented in this thesis.

In these experiments, we show that this framework for studying 2D BECs in a rotating frame perturbed by varying optical and magnetic potentials provides opportunities to observe interesting turbulent behavior. We induce this turbulent behavior by creating differential rotation. We explore two main methods of developing that rotational velocity gradient. The bulk of the study looks at stirring from the inside and outside of the condensate at a rotation rate that varies from the background reference frame by rotating the eccentric trap and eccentric laser. The end of the study looks at an attempt to directly form “jet-like” behavior similar to the behavior observed in *A Laboratory Model of Saturn’s Polar Hexagon* [3] with an annular laser shape.

In Chapter 4, we will look at the other analytical methods developed and explored; however, for this data section we will only compare the results of data sets via visual inspection since it was applied to all data sets. Other analytical methods were not universally applied to all of the data for many reasons: being qualitative, being developed later in the study, having long calculation times, being difficult to verify, or having tentative or inconclusive results. Primarily, we will look to see that the data is not simply a slight agitation or rotation of a vortex lattice, but

instead shows significant indicators of turbulence. The main indicators we will look for via visual inspection are grouping of the vortices which may indicate the development of characteristic structures from turbulence and radial motion of the vortices which may indicate large structural rotation of vortices from turbulence.

Before going into the data sets, a brief reference for the constants and parameters are provided in the tables below.

Name of Constant	Symbol	Value
Relative atomic mass of ^{87}Rb	m	86.909184 amu
Atomic mass unit	amu	$1.66054 \cdot 10^{27}$ kg
Bohr radius	a_0	$5.29 \cdot 10^{-11}$ m
Reduced Planck's constant	\hbar	$1.0546 \cdot 10^{-34}$ kg \cdot m ² / s
Speed of light	c	2.998e8 m / s
Scattering length of ^{87}Rb	a_{scat}	$95.44 \cdot a_0$
Resonant frequency of ^{87}Rb D2 line	ω_{0Rb}	$2.415 \cdot 10^{15}$ s ⁻¹
Our choice of blue-detuned laser frequency	ω_l	$2.8541 \cdot 10^{15}$ s ⁻¹
Detuning	Δ_ω	$4.3909 \cdot 10^{14}$ s ⁻¹
Spontaneous Decay rate	A	$3.7071 \cdot 10^7$ s ⁻¹
Saturation intensity of ^{87}Rb	I_{sat}	16.2508 W/m ²

Table 3.1: Physical constants and parameters used in the simulation.

Variable Name	Variable Symbol
Experiment Number	$\#$
Abbreviated Experiment Name	$Name$
Laser Shape (Gaussian unless specified, ω_x & ω_y) (μm)	$Shape$
Laser Max Energy in units of Chemical Potential (μ)	E
Laser Rotation Frequency in the Rotating Frame (1/s)	ω_L
Frequency of the Rotating Frame (1/s)	ω_F
Eccentric Trap Rotation Frequency (1/s)	ω_T
Time-Step Duration (s)	Δt
Damping (unitless)	γ
Number of Atoms (atoms)	N
Eccentricity of Trap (unitless)	ε
Base Trap Frequency in the x -direction and y -direction (1/s)	ω_{\perp}
Trap Frequency in the z -direction (1/s)	ω_z
Experiment Duration (s)	t
Domain of Simulation in the x -direction and y -direction (μm)	D
Spatial Resolution (μm)	dx
Momentum Resolution ($\text{kg}\cdot\text{m/s}$)	dp

Table 3.2: Symbol definitions and their units relevant to our simulations.

The following tables, Table 3.3 through Table 3.9, show the experimental parameters for all experiments presented in the data section. Parameters of interest, mostly those being tried for the first time, are highlighted for convenience.

MATLAB Data Set 1					
#	1	2	3	4	5
Name	Low Damp.	Smaller Laser	Larger Laser	Smaller Freq.	Larger Freq.
Shape (μm)	12.5, 9.375	4.17, 3.125	25, 18.75	12.5, 9.375	12.5, 9.375
E (μ)	1.2	1.2	1.2	1.2	1.2
ω_L (1/s)	$2\pi(-1)$	$2\pi(-1)$	$2\pi(-1)$	$2\pi(-1/3)$	$2\pi(-3)$
ω_F (1/s)	$2\pi(10)$	$2\pi(10)$	$2\pi(10)$	$2\pi(10)$	$2\pi(10)$
ω_T (1/s)	$2\pi(-1)$	$2\pi(-1)$	$2\pi(-1)$	$2\pi(-1/3)$	$2\pi(-3)$
Δt (s)	3.91E-07	3.91E-07	3.91E-07	3.91E-07	3.91E-07
γ (unitless)	0.0003	0.0003	0.0003	0.0003	0.0003
N (atoms)	1.00E+06	1.00E+06	1.00E+06	1.00E+06	1.00E+06
ε (unitless)	-0.035725	-0.035725	-0.035725	-0.035725	-0.035725
ω_{\perp} (1/s)	$2\pi(11.11)$	$2\pi(11.11)$	$2\pi(11.11)$	$2\pi(11.11)$	$2\pi(11.11)$
ω_z (1/s)	$2\pi(427)$	$2\pi(427)$	$2\pi(427)$	$2\pi(427)$	$2\pi(427)$
t (s)	6.5	6.5	6.5	6.5	6.5
D (μm)	200	200	200	200	200
dx (μm)	0.3906	0.3906	0.3906	0.3906	0.3906
dp (kg·m/s)	3.31E-30	3.31E-30	3.31E-30	3.31E-30	3.31E-30

Table 3.3: Parameters for the first set of experiments. Dimensional units for the numbers of each row are given in parentheses in column one for Table 3.3 through Table 3.9. For tables after Table 3.9 (Table 3.10 through Table 3.34), dimensional units for the numbers of each column are given in parentheses in row one.

MATLAB Data Set 2				
#	1	2	3	4
Name	No Laser	Faster Freq.	Less Ecc.	Dimpled
Shape (μm)	N/A	12.5, 9.375	12.5, 9.375	25, 18.75
E (μ)	0	1.2	1.2	0.3
ω_L (1/s)	N/A	$2\pi(-9)$	$2\pi(-3)$	$2\pi(-3)$
ω_F (1/s)	$2\pi(10)$	$2\pi(10)$	$2\pi(10)$	$2\pi(10)$
ω_T (1/s)	$2\pi(-3)$	$2\pi(-9)$	$2\pi(-3)$	$2\pi(-3)$
Δt (s)	3.91E-07	3.91E-07	3.91E-07	3.91E-07
γ (unitless)	0.0003	0.0003	0.0003	0.0003
N (atoms)	1.00E+06	1.00E+06	1.00E+06	1.00E+06
ε (unitless)	-0.035725	-0.035725	-0.01190833	-0.035725
ω_{\perp} (1/s)	$2\pi(11.11)$	$2\pi(11.11)$	$2\pi(11.11)$	$2\pi(11.11)$
ω_z (1/s)	$2\pi(427)$	$2\pi(427)$	$2\pi(427)$	$2\pi(427)$
t (s)	6.5	6.5	6.5	6.5
D (μm)	200	200	200	200
dx (μm)	0.3906	0.3906	0.3906	0.3906
dp (kg·m/s)	3.31E-30	3.31E-30	3.31E-30	3.31E-30

Table 3.4: Parameters for the second set of experiments.

MATLAB Data Set 3				
#	1	2	3	4
Name	Larger Dimple	Round Dimple	Outer Round	Inner Round
Shape (μm)	50, 37.5	21.875, 21.875	25, 18.75	21.875, 21.875
E (μ)	0.3	0.3	0.3	0.3
ω_L (1/s)	$2\pi(-3)$	$2\pi(-3)$	$2\pi(-3)$	$2\pi(-3)$
ω_F (1/s)	$2\pi(10)$	$2\pi(10)$	$2\pi(10)$	$2\pi(10)$
ω_T (1/s)	$2\pi(-3)$	$2\pi(-3)$	$2\pi(-3)$	$2\pi(-3)$
Δt (s)	3.91E-07	3.91E-07	3.91E-07	3.91E-07
γ (unitless)	0.0003	0.0003	0.0003	0.0003
N (atoms)	1.00E+06	1.00E+06	1.00E+06	1.00E+06
ε (unitless)	-0.035725	0	0	-0.035725
ω_{\perp} (1/s)	$2\pi(11.11)$	$2\pi(11.11)$	$2\pi(11.11)$	$2\pi(11.11)$
ω_z (1/s)	$2\pi(427)$	$2\pi(427)$	$2\pi(427)$	$2\pi(427)$
t (s)	6.5	6.5	6.5	6.5
D (μm)	200	200	200	200
dx (μm)	0.3906	0.3906	0.3906	0.3906
dp (kg·m/s)	3.31E-30	3.31E-30	3.31E-30	3.31E-30

Table 3.5: Parameters for the third set of experiments.

MATLAB Data Set 4				
#	1	2	3	4
Name	Lower Ecc.	Alt. Rot.	Inner Alt.	Outer Alt.
Shape (μm)	22.13,21.61	22.66,21.09	22.66,21.09	22.66,21.09
E (μ)	0.3	0.3	0.3	0.3
ω_L (1/s)	$2\pi(-3)$	$2\pi(3)$	$2\pi(3)$	$2\pi(-3)$
ω_F (1/s)	$2\pi(10)$	$2\pi(10)$	$2\pi(10)$	$2\pi(10)$
ω_T (1/s)	$2\pi(-3)$	$2\pi(3)$	$2\pi(-3)$	$2\pi(3)$
Δt (s)	3.91E-07	3.91E-07	3.91E-07	3.91E-07
γ (unitless)	0.0003	0.0003	0.0003	0.0003
N (atoms)	1.00E+06	1.00E+06	1.00E+06	1.00E+06
ε (unitless)	-0.011908333	-0.035725	-0.035725	-0.035725
ω_{\perp} (1/s)	$2\pi(11.11)$	$2\pi(11.11)$	$2\pi(11.11)$	$2\pi(11.11)$
ω_z (1/s)	$2\pi(427)$	$2\pi(427)$	$2\pi(427)$	$2\pi(427)$
t (s)	6.5	6.5	6.5	6.5
D (μm)	200	200	200	200
dx (μm)	0.3906	0.3906	0.3906	0.3906
dp (kg·m/s)	3.31E-30	3.31E-30	3.31E-30	3.31E-30

Table 3.6: Parameters for the fourth set of experiments.

MATLAB Data Set 5			
#	1	2	3
Name	No Damp	Both Slow	Slow Frame
Shape (μm)	22.66,21.09	22.66,21.09	22.66,21.09
E (μ)	0.3	0.3	0.3
ω_L (1/s)	$2\pi(-3)$	$2\pi(-1)$	$2\pi(-3)$
ω_F (1/s)	$2\pi(10)$	$2\pi(3.33)$	$2\pi(3.33)$
ω_T (1/s)	$2\pi(-3)$	$2\pi(-1)$	$2\pi(-3)$
Δt (s)	3.91E-07	3.91E-07	3.91E-07
γ (unitless)	0	0.0003	0.0003
N (atoms)	1.00E+06	1.00E+06	1.00E+06
ε (unitless)	-0.035725	-0.035725	-0.035725
ω_{\perp} (1/s)	$2\pi(11.11)$	$2\pi(11.11)$	$2\pi(11.11)$
ω_z (1/s)	$2\pi(427)$	$2\pi(427)$	$2\pi(427)$
t (s)	6.5	6.5	6.5
D (μm)	200	200	200
dx (μm)	0.3906	0.3906	0.3906
dp (kg·m/s)	3.31E-30	3.31E-30	3.31E-30

Table 3.7: Parameters for the fifth set of experiments.

MATLAB Data Set 11				
#	1	2	3	4
Name	Gauss. Still	Gauss. Rot.	1/100 Rev.	1/10 Rev.
Shape (μm)	6, 3.6 gauss	6, 3.6 gauss	6, 3.6 gauss	6, 3.6 gauss
E (μ)	24	24	0.24	2.4
ω_L (1/s)	0	0.5	-0.5	-0.5
ω_F (1/s)	$2\pi(3.3)$	$2\pi(3.3)$	$2\pi(3.3)$	$2\pi(3.3)$
ω_T (1/s)	0	0	0	0
Δt (s)	3.91E-07	3.91E-07	3.91E-07	3.91E-07
γ (unitless)	0.0003	0.0003	0.0003	0.0003
N (atoms)	1.00E+06	1.00E+06	1.00E+06	1.00E+06
ε (unitless)	0	0	0	0
ω_{\perp} (1/s)	$2\pi(4.125)$	$2\pi(4.125)$	$2\pi(4.125)$	$2\pi(4.125)$
ω_z (1/s)	$2\pi(79.41)$	$2\pi(79.41)$	$2\pi(79.41)$	$2\pi(79.41)$
t (s)	17	17	17	17
D (μm)	400	400	400	400
dx (μm)	0.78125	0.78125	0.78125	0.78125
dp (kg·m/s)	1.66E-30	1.66E-30	1.66E-30	1.66E-30

Table 3.8: Parameters for the sixth set of experiments presented in this thesis. In the MATLAB data, this is set 11 as noted in the table. Here, “gauss” refers to the annular gaussian experiments first described in section 3.21, where the first number refers to the number of individual gaussian laser beams that make up the annulus and the second number refers to the size of the gaussian laser beams by their FWHM.

MATLAB Data Set 12	
#	1
Name	Speckled
Shape (μm)	Annulus, 4
E (μ)	0.8
ω_L (1/s)	0.5
ω_F (1/s)	$2\pi(3.3)$
ω_T (1/s)	0
Δt (s)	3.91E-07
γ (unitless)	0.0003
N (atoms)	1.00E+06
ε (unitless)	0
ω_{\perp} (1/s)	$2\pi(4.125)$
ω_z (1/s)	$2\pi(79.41)$
t (s)	17
D (μm)	400
dx (μm)	0.78125
dp (kg·m/s)	1.66E-30

Table 3.9: Parameters for the seventh set of experiments presented in this thesis. In the MATLAB data, this is set 12 as noted in the table. Here, “annulus,” means a superposition of gaussians with randomly assigned positions, widths, and depths with a mask applied to set the laser intensity inside a specified radius and outside of a specified radius to zero. The second number on that row indicates the width of the annulus.

For all images presented in this section, yellow represents high density and blue indicates low density.

3.1 Set 1 – Experiment 1 – Low Damping Baseline

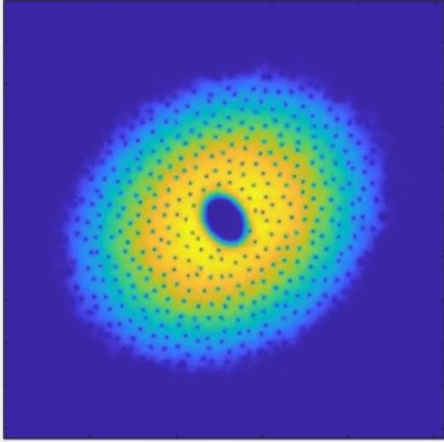


Figure 3.1: An image of the density of the condensate for set 1, experiment 1.

<i>Shape</i> (μm)	<i>E</i> (μ)	ω_L (1/s)	ω_F (1/s)	ω_T (1/s)	γ (unitless)	ε (unitless)	ω_{\perp} (1/s)	ω_z (1/s)	<i>t</i> (s)
12.5, 9.375	1.2	$2\pi(-1)$	$2\pi(10)$	$2\pi(-1)$	0.0003	-0.035725	$2\pi(11.11)$	$2\pi(427)$	6.5

Table 3.10: A shortened version of Table 3.3 for set 1, experiment 1.

This first experiment aims to find an optimal parameter for damping in the condensate. The damping numerically describes the effect that the rotating frame has on the condensate. If the damping is too high, little motion of the vortices is observed. A low damping baseline is established in this simulation.

After manipulating the damping coefficient, a value was found that allows relative movement of the vortices. The movement expected was some stirring and clustering of the vortices in the band between the inner laser and the outer bounds of the rotating magnetic trap. This movement is observed but does not appear in a predictable pattern.

3.2 Set 1 – Experiment 2 – Smaller Laser

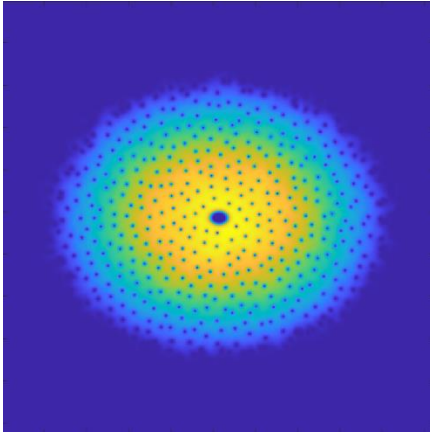


Figure 3.2: An image of the density of the condensate for set 1, experiment 2.

<i>Shape</i> (μm)	<i>E</i> (μ)	ω_L (1/s)	ω_F (1/s)	ω_T (1/s)	γ (unitless)	ε (unitless)	ω_{\perp} (1/s)	ω_z (1/s)	<i>t</i> (s)
4.17, 3.125	1.2	$2\pi(-1)$	$2\pi(10)$	$2\pi(-1)$	0.0003	-0.035725	$2\pi(11.11)$	$2\pi(427)$	6.5

Table 3.11: A shortened version of Table 3.3 for set 1, experiment 2.

This experiment aims to find an optimal parameter for laser diameter in the condensate. The goal of having an inner and outer rotating mechanism is to create a differential rotation. The question this experiment is trying to probe at is “how does the size of the laser affect the differential rotation?”

The smaller laser takes less time to settle into a relatively steady state than other experiments as the laser no longer seems to affect the behavior of the vortices. In this experiment, the effect of the eccentric rotating trap can be more readily seen. Vortices near the edge are strongly guided radially by the rotating eccentric trap. When compressed and expanded, some grouping and rotation of this grouping is observed.

3.3 Set 1 – Experiment 3 – Bigger Laser

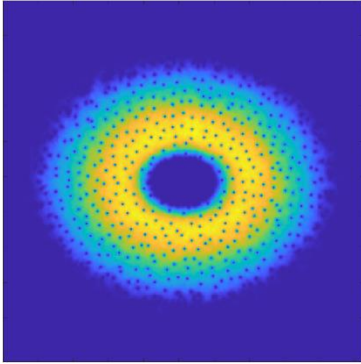


Figure 3.3: An image of the density of the condensate for set 1, experiment 3.

<i>Shape</i> (μm)	<i>E</i> (μ)	ω_L (1/s)	ω_F (1/s)	ω_T (1/s)	γ (unitless)	ε (unitless)	ω_{\perp} (1/s)	ω_z (1/s)	<i>t</i> (s)
25, 18.75	1.2	$2\pi(-1)$	$2\pi(10)$	$2\pi(-1)$	0.0003	-0.035725	$2\pi(11.11)$	$2\pi(427)$	6.5

Table 3.12: A shortened version of Table 3.3 for set 1, experiment 3.

The purpose of this experiment is to further investigate the effect of laser diameter on the system. We would like to know what effects a larger laser diameter might have on the behavior observed in the condensate.

A larger laser increased the amount of radial motion and grouping of vortices. The rotation rate of the grouped vortices seemed to increase, and the distance between vortices in an associated group seemed to increase. These metrics seem to point to increased instability in the fluid flow of the condensate and potentially indicate a transition from smaller, localized, instabilities, to larger instable flow patterns. Compression between inner and outer barriers from the larger laser may account for this change in behavior.

3.4 Set 1 – Experiment 4 – Smaller Frequency

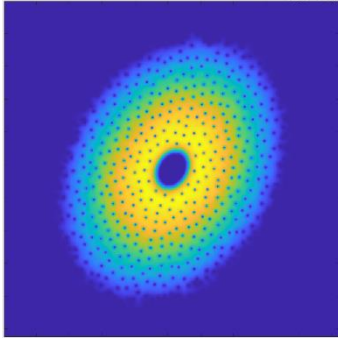


Figure 3.4: An image of the density of the condensate for set 1, experiment 4.

<i>Shape</i> (μm)	<i>E</i> (μ)	ω_L (1/s)	ω_F (1/s)	ω_T (1/s)	γ (unitless)	ε (unitless)	ω_{\perp} (1/s)	ω_z (1/s)	<i>t</i> (s)
12.5, 9.375	1.2	$2\pi(-1/3)$	$2\pi(10)$	$2\pi(-1/3)$	0.0003	-0.035725	$2\pi(11.11)$	$2\pi(427)$	6.5

Table 3.13: A shortened version of Table 3.3 for set 1, experiment 4.

This is the first experiment looking into the effect that the relative rotation of the trap and the laser have on the fluid flow dynamics of the condensate. We would like to know how strongly this rotation rate affects the fluid flow of the system. We think that this parameter could strongly influence the behavior of fluid flow as it directly controls the maximum potential for rotational velocity gradient.

This experiment showed that the relative rotation rate of the trap and the laser is important to the fluid flow dynamics. The slower rate of rotation resulted in a lower number of vortices per group, less radial motion of the vortices, and smaller effective size of groups of vortices. These have been flagged as indicators of less instability in the condensate, and we are not expecting to observe desired fluid flow behaviors from frequencies that are too low.

3.5 Set 1 – Experiment 5 – Larger Frequency

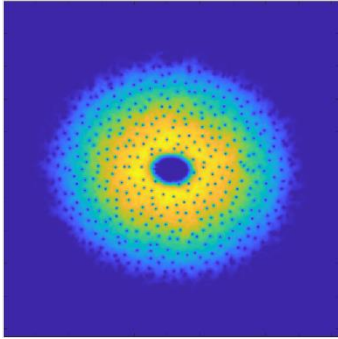


Figure 3.5: An image of the density of the condensate for set 1, experiment 5.

<i>Shape</i> (μm)	<i>E</i> (μ)	ω_L (1/s)	ω_F (1/s)	ω_T (1/s)	γ (unitless)	ε (unitless)	ω_{\perp} (1/s)	ω_z (1/s)	<i>t</i> (s)
12.5, 9.375	1.2	$2\pi(-3)$	$2\pi(10)$	$2\pi(-3)$	0.0003	-0.035725	$2\pi(11.11)$	$2\pi(427)$	6.5

Table 3.14: A shortened version of Table 3.3 for set 1, experiment 4.

This is the second experiment looking into the effect that the relative rotation of the trap and the laser have on the fluid flow dynamics of the condensate. We would like to know how strongly this rotation rate affects the fluid flow of the system. We think that this parameter could strongly influence the behavior of fluid flow as it directly controls the maximum potential for rotational velocity gradient.

The faster rate of rotation resulted in a higher number of vortices per group, more radial motion of the vortices, and larger observed size of groups of vortices. These seem to indicate more instability in the condensate, and there were no observed drawbacks to running at this higher frequency; however, we would like to see these behaviors become stable with respect to angle and a faster relative frequency may deter the formation of those structures.

3.6 Set 2 – Experiment 1 – No Laser

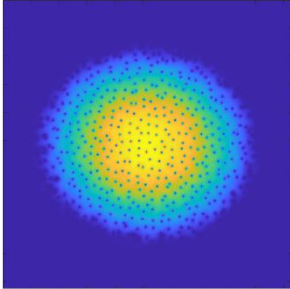


Figure 3.6: An image of the density of the condensate for set 2, experiment 1.

<i>Shape</i> (μm)	<i>E</i> (μ)	ω_L (1/s)	ω_F (1/s)	ω_T (1/s)	γ (unitless)	ε (unitless)	ω_{\perp} (1/s)	ω_z (1/s)	<i>t</i> (s)
N/A	0	N/A	$2\pi(10)$	$2\pi(-3)$	0.0003	-0.0357	$2\pi(11.11)$	$2\pi(427)$	6.5

Table 3.15: A shortened version of Table 3.4 for set 2, experiment 1.

This experiment aims to develop a better understanding of the rotating eccentric trap. We saw from the “Smaller Laser” experiment that the expansion and compression of the rotating trap strongly guided the behavior of vortices in the radial direction. This experiment aims to isolate that behavior from the laser.

Some aspects of the faster rotation rate from “Larger Frequency” can be seen as there is still some radial motion and grouping of the vortices. We expected to see less of the vortex grouping behavior as the inner laser seems to provide a compression that drives more grouping of the radially moving vortices. This expectation is observed and where there is some motion of the vortices towards the center, they do not seem to strongly affect the motion of the rest of the condensate. For these reasons, it seems like the inner laser is desirable for driving instabilities in the condensate.

3.7 Set 2 – Experiment 2 – Faster Frequency

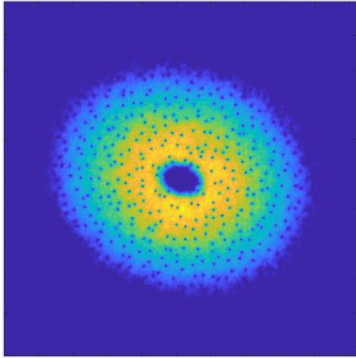


Figure 3.7: An image of the density of the condensate for set 2, experiment 2.

<i>Shape</i> (μm)	E (μ)	ω_L (1/s)	ω_F (1/s)	ω_T (1/s)	γ (unitless)	ε (unitless)	ω_{\perp} (1/s)	ω_z (1/s)	t (s)
12.5, 9.375	1.2	$2\pi(-9)$	$2\pi(10)$	$2\pi(-9)$	0.0003	-0.0357	$2\pi(11.11)$	$2\pi(427)$	6.5

Table 3.16: A shortened version of Table 3.4 for set 2, experiment 2.

The purpose of this experiment is to explore the upper range of reasonable frequencies for the rotation of the inner laser and the outer trap. Based on previous experiments, a larger rotational frequency seems to result in a higher gradient of differential rotation and thus more instability of vortex locations. We'd like to see what happens when the frequency is increased again.

The faster frequency seems to be too fast to drive the radial motion of vortices near the edge of the condensate. The overall effect seems to be a reduction in vortex positional instability. A different kind of turbulence is observed as noise builds up closer to the middle of the condensate, increasing towards the end of the simulation and indicating a limit on this simulation method.

3.8 Set 2 – Experiment 3 – Less Eccentric Trap

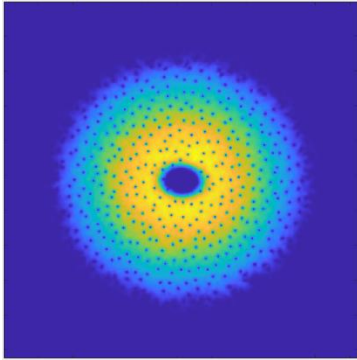


Figure 3.8: An image of the density of the condensate for set 2, experiment 3.

<i>Shape</i> (μm)	<i>E</i> (μ)	ω_L (1/s)	ω_F (1/s)	ω_T (1/s)	γ (unitless)	ε (unitless)	ω_{\perp} (1/s)	ω_z (1/s)	<i>t</i> (s)
12.5, 9.375	1.2	$2\pi(-3)$	$2\pi(10)$	$2\pi(-3)$	0.0003	-0.0119	$2\pi(11.11)$	$2\pi(427)$	6.5

Table 3.17: A shortened version of Table 3.4 for set 2, experiment 3.

The eccentricity of the trap is an interesting parameter because it does not have an analogous parameter in classical experiments of the same kind. In classical experiments the friction of a circular container can provide a stirring mechanism from the outside. The goal of this experiment is to probe the importance and effects of this parameter without changing the laser.

The lower eccentricity of the trap seems to drive the outer vortices less. More of the instability of vortex position seems to happen closer to the laser. There also seems to be less motion of vortices from the inner portion of the condensate towards the edge. Overall, these effects are relatively subtle when compared to other parameters explored so far.

3.9 Set 2 – Experiment 4 – Dimpled Condensate

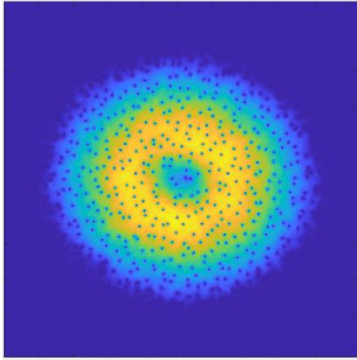


Figure 3.9: An image of the density of the condensate for set 2, experiment 4.

<i>Shape</i> (μm)	<i>E</i> (μ)	ω_L (1/s)	ω_F (1/s)	ω_T (1/s)	γ (unitless)	ε (unitless)	ω_{\perp} (1/s)	ω_z (1/s)	<i>t</i> (s)
25, 18.75	0.3	$2\pi(-3)$	$2\pi(10)$	$2\pi(-3)$	0.0003	-0.0357	$2\pi(11.11)$	$2\pi(427)$	6.5

Table 3.18: A shortened version of Table 3.4 for set 2, experiment 4.

We noticed interesting dynamics seem to happen near the laser and hypothesized that by reducing intensity of the laser, it may be easier to see vortex dynamics in and around that part of the condensate. When the laser is not pinning the vortices, they are trackable by eye.

This experiment had the most interesting results by far. Many groups of three vortices can be observed and they would often spin out from the middle of the condensate towards the edge. As these tightly grouped vortices spun towards the edge, they would interact with and group with more vortices. Sometimes, groups of 7 vortices can be seen temporarily all rotating together. This was the largest amount of grouping, grouped rotation, and radial motion of vortices seen so far.

3.10 Set 3 – Experiment 1 – Larger Dimple

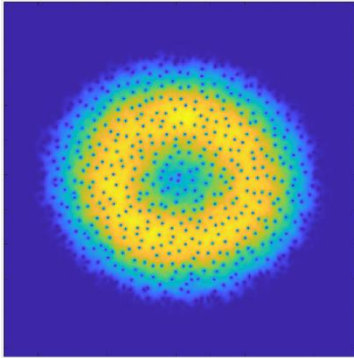


Figure 3.10: An image of the density of the condensate for set 3, experiment 1.

<i>Shape</i> (μm)	<i>E</i> (μ)	ω_L (1/s)	ω_F (1/s)	ω_T (1/s)	γ (unitless)	ε (unitless)	ω_{\perp} (1/s)	ω_z (1/s)	<i>t</i> (s)
50, 37.5	0.3	$2\pi(-3)$	$2\pi(10)$	$2\pi(-3)$	0.0003	-0.0357	$2\pi(11.11)$	$2\pi(427)$	6.5

Table 3.19: A shortened version of Table 3.5 for set 3, experiment 1.

The first dimple experiment elicited some of the most interesting behavior so far in the research. The purpose of this experiment is to try to understand what aspects of the dimpled laser led to the more interesting behavior. In this experiment we attempt to expand the transition zone from laser to no-laser in the condensate by expanding the diameter of the laser by a factor of two.

The first thing to notice is that the condensate took much longer to get into a relatively steady state. Many of the observations from the earlier dimpled experiment are observed; however, the groupings are not as tight, and the rotation rate of those groups is also lower. It's possible that spatially larger groups are formed but the distance between vortices is larger so that it is difficult to confirm without a more rigorous analytical method.

3.11 Set 3 – Experiment 2 – Dimpled, Round Trap and Laser

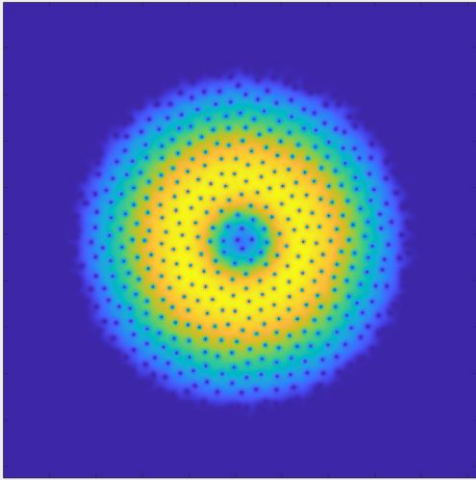


Figure 3.11: An image of the density of the condensate for set 3, experiment 2.

<i>Shape</i> (μm)	<i>E</i> (μ)	ω_L (1/s)	ω_F (1/s)	ω_T (1/s)	γ (unitless)	ε (unitless)	ω_{\perp} (1/s)	ω_z (1/s)	<i>t</i> (s)
21.875, 21.875	0.3	$2\pi(-3)$	$2\pi(10)$	$2\pi(-3)$	0.0003	0	$2\pi(11.11)$	$2\pi(427)$	6.5

Table 3.20: A shortened version of Table 3.5 for set 3, experiment 2.

We would like to show that the relative difference in rotation rates is the driving mechanism for instability in the condensate. Currently, the relative rotational difference is created by making eccentric potentials in the condensate and rotating them at some rate relative to the background rotation of the reference frame. This experiment removes that eccentricity both to serve as a control for the stirring and to observe the effects, if any, the dimple has on the condensate independent of the stirring mechanism.

Although there is some instability observed, the condensate appears to be better described as a slight disturbance from the rotational ground state. The vortices remain mostly in place.

3.12 Set 3 – Experiment 3 – Dimpled, Round Trap

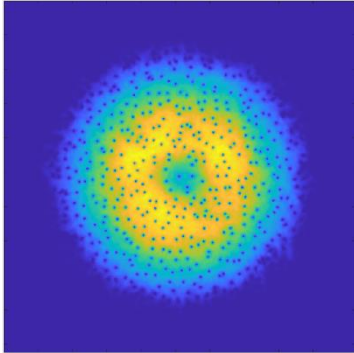


Figure 3.12: An image of the density of the condensate for set 3, experiment 3.

<i>Shape</i> (μm)	<i>E</i> (μ)	ω_L (1/s)	ω_F (1/s)	ω_T (1/s)	γ (unitless)	ε (unitless)	ω_{\perp} (1/s)	ω_z (1/s)	<i>t</i> (s)
25, 18.75	0.3	$2\pi(-3)$	$2\pi(10)$	$2\pi(-3)$	0.0003	0	$2\pi(11.11)$	$2\pi(427)$	6.5

Table 3.21: A shortened version of Table 3.5 for set 3, experiment 3.

This experiment is an expansion of the study of the role of the stirring mechanisms used to create a differential rotation. For this experiment, the eccentricity of the trap is removed to isolate the effect of the rotating eccentric laser.

Many of the main behaviors observed in the original “Dimpled Condensate” experiment are observed. It’s possible that there are more small groups of vortices (2 or 3 vortices) or that those small groups that originate near the center of the condensate last longer as they travel towards the outer edge of the condensate; however, this tentative observation is quite subtle and requires a more rigorous analytical method to confirm.

3.13 Set 3 – Experiment 4 – Dimpled, Round Laser

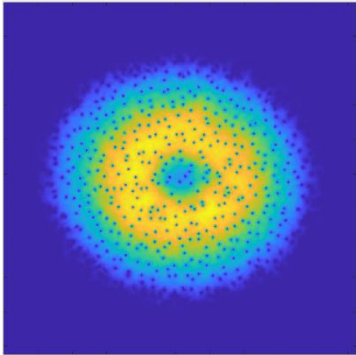


Figure 3.13: An image of the density of the condensate for set 3, experiment 4.

<i>Shape</i> (μm)	<i>E</i> (μ)	ω_L (1/s)	ω_F (1/s)	ω_T (1/s)	γ (unitless)	ε (unitless)	ω_{\perp} (1/s)	ω_z (1/s)	<i>t</i> (s)
21.875, 21.875	0.3	$2\pi(-3)$	$2\pi(10)$	$2\pi(-3)$	0.0003	-0.0357	$2\pi(11.11)$	$2\pi(427)$	6.5

Table 3.22: A shortened version of Table 3.5 for set 3, experiment 4.

This experiment is an expansion of the study of the role of the stirring mechanisms used to create a differential rotation. For this experiment, the eccentricity of the laser is removed to isolate the effect of the rotating eccentric trap.

Many of the main behaviors observed in the original “Dimpled Condensate” experiment are observed. It’s possible that there are larger groups of vortices; however, this tentative observation is quite subtle and requires a more rigorous analytical method to confirm. The larger conclusion drawn from this set is that the eccentric rotating stirring does create these instabilities, but whether that comes from the laser or the trap or both is much less important.

3.14 Set 4 – Experiment 1 – Dimpled with Lower Eccentricity

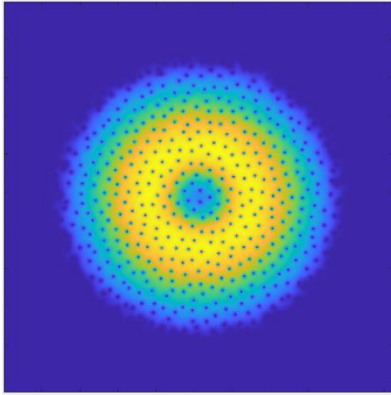


Figure 3.14: An image of the density of the condensate for set 4, experiment 1.

<i>Shape</i> (μm)	<i>E</i> (μ)	ω_L (1/s)	ω_F (1/s)	ω_T (1/s)	γ (unitless)	ε (unitless)	ω_{\perp} (1/s)	ω_z (1/s)	<i>t</i> (s)
22.13, 21.61	0.3	$2\pi(-3)$	$2\pi(10)$	$2\pi(-3)$	0.0003	-0.0119	$2\pi(11.11)$	$2\pi(427)$	6.5

Table 3.23: A shortened version of Table 3.6 for set 4, experiment 1.

This experiment was designed to further explore the role of the rotating mechanism on the condensate, specifically in the case of a dimpled laser. This is the final part of the study from set 3 into the eccentric rotating mechanism. In this case, rather than the eccentricity we were using earlier or perfectly round potentials, this experiment looks at a situation with a non-zero, reduced eccentricity.

This simulation was similar in result to that of the perfectly round trap and laser. The effect of the driving mechanism was mostly or entirely nullified at this eccentricity. There was little positional instability of the vortices.

3.15 Set 4 – Experiment 2 – Dimpled with Alternate Rotation

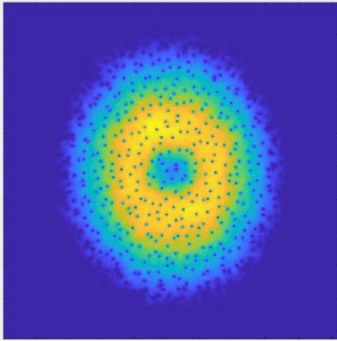


Figure 3.15: An image of the density of the condensate for set 4, experiment 2.

<i>Shape</i> (μm)	<i>E</i> (μ)	ω_L (1/s)	ω_F (1/s)	ω_T (1/s)	γ (unitless)	ε (unitless)	ω_{\perp} (1/s)	ω_z (1/s)	<i>t</i> (s)
22.66, 21.09	0.3	$2\pi(3)$	$2\pi(10)$	$2\pi(3)$	0.0003	-0.0357	$2\pi(11.11)$	$2\pi(427)$	6.5

Table 3.24: A shortened version of Table 3.6 for set 4, experiment 2.

The purpose of this experiment is to probe the effects of relative rotation with the reference frame compared to having relative rotation against the reference frame. In this set, we will also look at the trap and laser rotating in different directions to see that effect as well.

This simulation was similar in result to that of the “Dimpled Condensate” experiment from set 2, experiment 4. There may be differences, but they would require a more rigorous analytical approach to confirm. The main conclusion that can be drawn from this experiment is that the alternate rotation did not seem to have the same amount of influence as other parameters explored in this study.

3.16 Set 4 – Experiment 3 – Dimpled, Alternate Laser Rotation

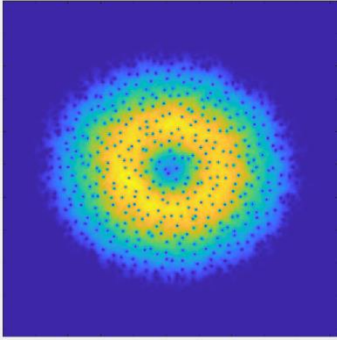


Figure 3.16: An image of the density of the condensate for set 4, experiment 3.

<i>Shape</i> (μm)	<i>E</i> (μ)	ω_L (1/s)	ω_F (1/s)	ω_T (1/s)	γ (unitless)	ε (unitless)	ω_{\perp} (1/s)	ω_z (1/s)	<i>t</i> (s)
22.66, 21.09	0.3	$2\pi(3)$	$2\pi(10)$	$2\pi(-3)$	0.0003	-0.0357	$2\pi(11.11)$	$2\pi(427)$	6.5

Table 3.25: A shortened version of Table 3.6 for set 4, experiment 3.

This experiment is an expansion in the study of the rotation directions of the trap and the laser with respect to the reference frame. In this experiment, we flip the polarity of rotation frequency of just the laser. In this case, one of the potentials is going slower than the reference frame and the other is going faster. This is an interesting case because it allows for double the maximum differential rotation without increasing the trap frequency further which failed to produce good results in “Faster Frequency” from set 2, experiment 2.

There seems to be more rapid movement and grouping of vortices than in prior dimpled experiments, but a more rigorous analytical method is needed to confirm this observation.

3.17 Set 4 – Experiment 4 – Dimpled, Alternate Trap Rotation

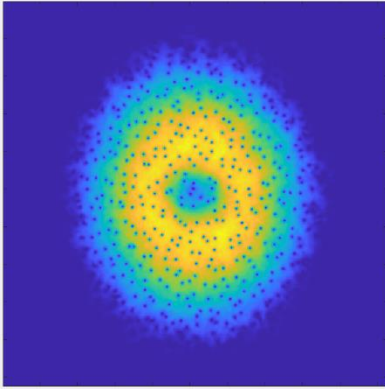


Figure 3.17: An image of the density of the condensate for set 4, experiment 4.

<i>Shape</i> (μm)	<i>E</i> (μ)	ω_L (1/s)	ω_F (1/s)	ω_T (1/s)	γ (unitless)	ε (unitless)	ω_{\perp} (1/s)	ω_z (1/s)	<i>t</i> (s)
22.66, 21.09	0.3	$2\pi(3)$	$2\pi(10)$	$2\pi(-3)$	0.0003	-0.0357	$2\pi(11.11)$	$2\pi(427)$	6.5

Table 3.26: A shortened version of Table 3.6 for set 4, experiment 4.

Similar to the previous experiment, we are looking at the effect on the condensate when one of the eccentric potentials is rotating in a different direction than the other. In this experiment, we flip the polarity of the rotational frequency of just the trap.

There seems to be more rapid movement and grouping of vortices than in prior dimpled experiments, and there seems to be a slight difference in position of that behavior from set 4, experiment 3. The increased rapid movement and grouping of vortices seems to be closer to the edge of the condensate than the previous experiment. Which potential is working against the reference frame does seem to have an impact on the observed behavior.

3.18 Set 5 – Experiment 1 – No Damping

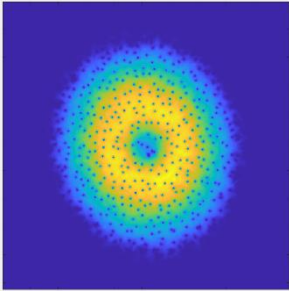


Figure 3.18: An image of the density of the condensate for set 5, experiment 1.

<i>Shape</i> (μm)	<i>E</i> (μ)	ω_L (1/s)	ω_F (1/s)	ω_T (1/s)	γ (unitless)	ε (unitless)	ω_{\perp} (1/s)	ω_z (1/s)	<i>t</i> (s)
22.66, 21.09	0.3	$2\pi(-3)$	$2\pi(10)$	$2\pi(-3)$	0	-0.0357	$2\pi(11.11)$	$2\pi(427)$	6.5

Table 3.27: A shortened version of Table 3.7 for set 5, experiment 1.

Up to this point, we have used the same damping constant that we optimized for in the first experiment of the first set “Low Damping Baseline.” Noting that the damping is already very low, we’d like to know how much of observed behavior is dependent on the damping coefficient. The damping coefficient is damping to the rotating frame. In other words, we’d like to know how important the coupling is to that rotating frame. In this experiment we will gradually drop the damping down to zero to observe any effects that occur as the damping is lower and eventually removed.

The condensate eventually breaks up; but before that, no interesting differences in behavior of the condensate are observed.

3.19 Set 5 – Experiment 2 – Rotating Frame and Stirring Slowed

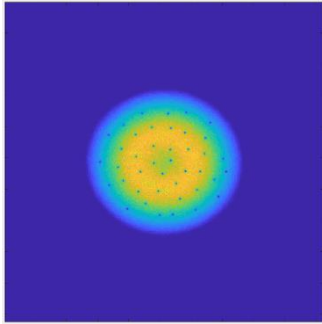


Figure 3.19: An image of the density of the condensate for set 5, experiment 2.

<i>Shape</i> (μm)	<i>E</i> (μ)	ω_L (1/s)	ω_F (1/s)	ω_T (1/s)	γ (unitless)	ε (unitless)	ω_{\perp} (1/s)	ω_z (1/s)	<i>t</i> (s)
22.66, 21.09	0.3	$2\pi(-1)$	$2\pi(3.33)$	$2\pi(-1)$	0.0003	-0.0357	$2\pi(11.11)$	$2\pi(427)$	6.5

Table 3.28: A shortened version of Table 3.7 for set 5, experiment 2.

In further exploration of the role of the rotating frame on the condensate, we now look at the role of the rotating frame on the simulation. For the first time, we change the rotating frame rate, lowering all of the rotation rates by a factor of 3. We would like to see if behaviors we've seen so far are invariant to scale of the rotation rates, and what other effects might come about from these changes.

There is some motion of the vortices is observed, but besides being vaguely rotational at what seems to be about the rate of the rotating eccentric trap, little else is observed. There is no distinguishable grouping of vortices in space.

3.20 Set 5 – Experiment 3 – Rotating Frame Slowed

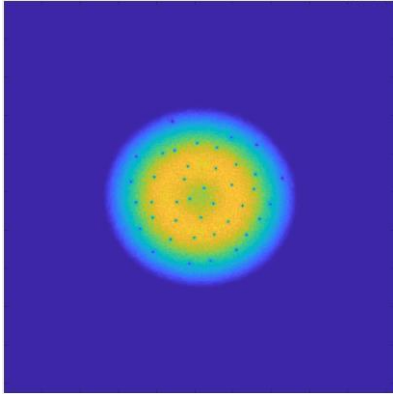


Figure 3.20: An image of the density of the condensate for set 5, experiment 3.

<i>Shape</i> (μm)	<i>E</i> (μ)	ω_L (1/s)	ω_F (1/s)	ω_T (1/s)	γ (unitless)	ε (unitless)	ω_{\perp} (1/s)	ω_z (1/s)	<i>t</i> (s)
22.66, 21.09	0.3	$2\pi(-3)$	$2\pi(3.33)$	$2\pi(-3)$	0.0003	-0.0357	$2\pi(11.11)$	$2\pi(427)$	6.5

Table 3.29: A shortened version of Table 3.7 for set 5, experiment 3.

This is an expansion into the study on the role of the rotating frame's rotation rate on the behaviors observed so far in the condensate. In this experiment we slow down the rotation rate of the rotating frame without changing the rotation rate of the stirring mechanisms of the laser and the trap.

Little motion of the vortices is observed, and there is no distinguishable grouping of vortices in space. Similar to the previous experiment in the set, it does not seem to be possible to see the same interesting behaviors with this slowed rotation rate. The rotating frame's rotation rate seems to be a very important parameter for this study.

3.21 Set 11 – Experiment 1 – 6 Still Gaussian Lasers

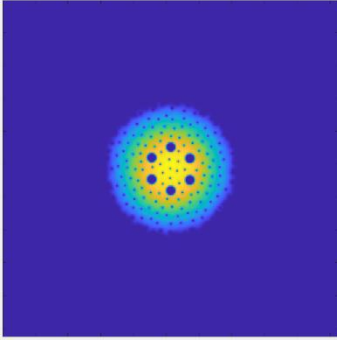


Figure 3.21: An image of the density of the condensate for set 11, experiment 1.

<i>Shape</i> (μm)	<i>E</i> (μ)	ω_L (1/s)	ω_F (1/s)	ω_T (1/s)	γ (unitless)	ε (unitless)	ω_{\perp} (1/s)	ω_z (1/s)	<i>t</i> (s)
6, 3.6 gauss	24	0	$2\pi(3.3)$	0	0.0003	0	$2\pi(4.125)$	$2\pi(79.41)$	17

Table 3.30: A shortened version of Table 3.8 for set 11, experiment 1.

In previous experiments throughout this study, the mechanism used to differential rotation was rotating eccentric potentials on the inside and outside of the condensate. In this set, we will attempt to create a jet of fluid flow in the condensate by rotating a series of gaussians at some radius between the center and edge of the condensate. This first experiment in the set will act as a control with the gaussian laser beams still in the condensate.

Not much motion of the vortices is observed after the condensate reaches a relatively steady state. This was the expected outcome of the control experiment.

3.22 Set 11 – Experiment 2 – 6 Rotating Gaussian Lasers

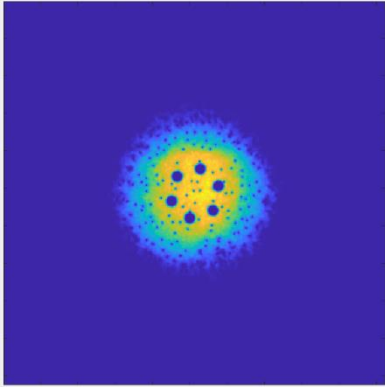


Figure 3.22: An image of the density of the condensate for set 11, experiment 2.

<i>Shape</i> (μm)	<i>E</i> (μ)	ω_L (1/s)	ω_F (1/s)	ω_T (1/s)	γ (unitless)	ε (unitless)	ω_{\perp} (1/s)	ω_z (1/s)	<i>t</i> (s)
6, 3.6 gauss	24	0.5	$2\pi(3.3)$	0	0.0003	0	$2\pi(4.125)$	$2\pi(79.41)$	17

Table 3.31: A shortened version of Table 3.8 for set 11, experiment 2.

The aim of the experiment is to find evidence that creating a jet-like fluid flow in the condensate is possible with this method of perturbation. We'd also like to study the effects of that jet, should it form. If this jet is formed, and our hypothesis about the velocity gradient causing instability of vortex position is correct, we should see dramatic radial motion of the vortices.

Eddy-like behavior is observed around the lasers. Vortices near the radius of the lasers move with the direction of the lasers and vortices further out move in the opposite direction. Many vortices move radially between these two zones changing their rotational direction as they cross.

3.23 Set 11 – Experiment 3 – Much Less Laser Power, Reversed

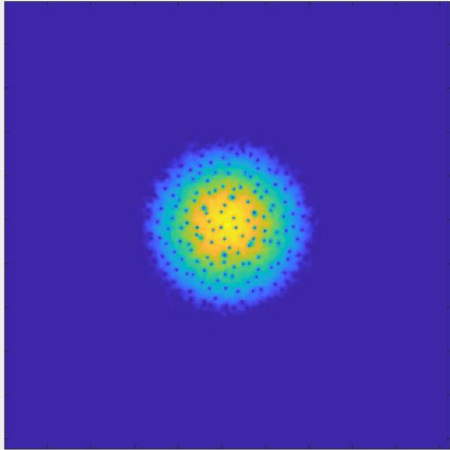


Figure 3.23: An image of the density of the condensate for set 11, experiment 3.

<i>Shape</i> (μm)	<i>E</i> (μ)	ω_L (1/s)	ω_F (1/s)	ω_T (1/s)	γ (unitless)	ε (unitless)	ω_{\perp} (1/s)	ω_z (1/s)	<i>t</i> (s)
6, 3.6 gauss	0.24	-0.5	$2\pi(3.3)$	0	0.0003	0	$2\pi(4.125)$	$2\pi(79.41)$	17

Table 3.32: A shortened version of Table 3.8 for set 11, experiment 3.

The goal of this experiment is to find the importance of laser power and direction of rotation of the lasers on the behavior observed in “6 Rotating Gaussian Lasers” from set 11, experiment 2. Laser power will simultaneously increase the amount of condensate pushed away and the effective area from which it is pushed.

Some of the behavior from the previous experiment is observed, but to a much lesser extent. Some vortices show eddy-like motion, but it is not as consistent as in the earlier experiment. Little more can be conclusively stated without a more rigorous analytical method.

3.24 Set 11 – Experiment 4 –Less Laser Power, Reversed

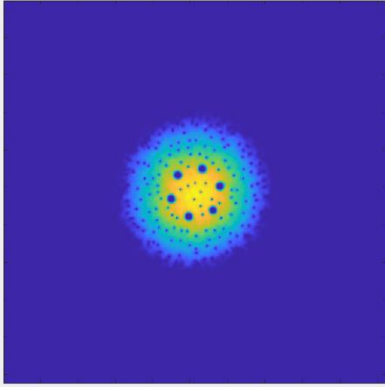


Figure 3.24: An image of the density of the condensate for set 11, experiment 4.

<i>Shape</i> (μm)	<i>E</i> (μ)	ω_L (1/s)	ω_F (1/s)	ω_T (1/s)	γ (unitless)	ε (unitless)	ω_{\perp} (1/s)	ω_z (1/s)	<i>t</i> (s)
6, 3.6 gauss	2.4	-0.5	$2\pi(3.3)$	0	0.0003	0	$2\pi(4.125)$	$2\pi(79.41)$	17

Table 3.33: A shortened version of Table 3.8 for set 11, experiment 4.

We hypothesize that the previous experiment had a laser power that was too low, and we aim to see more of the behavior from “6 Rotating Gaussian Lasers” in set 11, experiment 2 by raising the laser power from the previous experiment by a factor of 10. We also hope to see with this increase whether the change in rotation direction has had an effect when compared to set 11, experiment 2.

With the higher laser power, it seems evident that the reversed rotation direction suppresses the eddy-like behavior. As the simulation got later into a steady state, eddy-like behavior was seen less often and eddies that did appear were quickly stopped.

3.25 Set 12 – Experiment 1 –Speckled Annulus

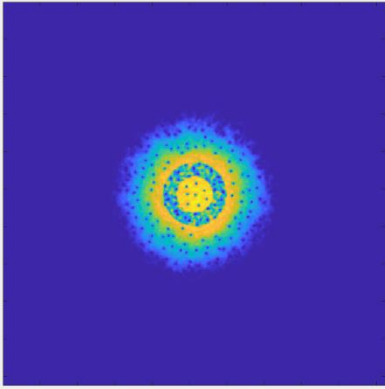


Figure 3.25: An image of the density of the condensate for set 12, experiment 1.

<i>Shape</i> (μm)	<i>E</i> (μ)	ω_L (1/s)	ω_F (1/s)	ω_T (1/s)	γ (unitless)	ε (unitless)	ω_{\perp} (1/s)	ω_z (1/s)	<i>t</i> (s)
Annulus, 4	0.8	0.5	$2\pi(3.3)$	0	0.0003	0	$2\pi(4.125)$	$2\pi(79.41)$	17

Table 3.34: A shortened version of Table 3.9 for set 12, experiment 1.

The purpose of this experiment is to isolate the jet-flow and eddy-like behavior from the Gaussian lasers used in the previous sets. We will attempt to do this by replacing the 6 Gaussian lasers with a super-position of gaussians of different depths and widths. The combination is a random speckle pattern used as a rough surface to stir the condensate.

The eddy-like and jet-like behaviors are seen just as in “6 Rotating Gaussian Lasers” from set 11, experiment 2, but the behavior is more consistent. Where the comparing experiment had strong dependence on the gaussian location, the behaviors here seem to happen at any angle.

3.26 Missing Sets 6-10

Several sets of data have been omitted from this paper. A brief explanation of those sets and why they were omitted will be presented here.

3.26.1 Set 6 – Much Larger Dimples

Interest was growing in the behavior of vortices along the edge of the dimple. To expand that region in area and circumference, the dimple diameters were expanded up to 16x the original laser diameter. Larger laser diameters pushed the condensate towards the edges of the spatial domain. It was shown that insufficient spatial domain caused errors with the Fourier transform methods used in the time-step evolution. A correction could have been made to recalculate without this issue, but the increased computation time was evaluated not to be worth the limited change in behavior observed. For this reason, this set was omitted.

3.26.2 Set 7 – Stronger Damping and Different Stirring Rates

There were nine experiments conducted looking at damping and stirring rates. Higher damping rates just seemed to reduce instability and the different stirring rates were not identifiably different in behavior without better analytical techniques. For this reason, this set was omitted.

3.26.3 Set 8 – Computation Timing

Set 8 contained the calculation of ground states used as a comparison to other calculation methods used by other scientists. The other calculation methods were not deemed significantly faster or more accurate than the current method and were not explored further. For this reason, this set was omitted.

3.26.4 Set 9 – Laser Convolution

Polygonal laser shapes were formed with smaller rotating eccentric gaussians. This method took a lot of computation time, and the condensate was breaking up too early. With adjustments, the condensate started to last long enough to get an idea of what might happen, but it did not seem to be in the same direction as our current study and the method was abandoned. For this reason, this set was omitted.

3.26.5 Set 10 – Polygonal Boundaries

A polygonal barrier at the edge of the condensate was explored. This method took some effort to get working; and when it was finally close to working, it became apparent that the barrier by itself did not initiate any particularly interesting behavior in the condensate. In the future, this idea could be explored further with round, quasi-round, or rough-round boundaries in conjunction with other ideas put forward in this paper. That might create some interesting effects, especially when considering that this boundary could rotate with or against other stirring mechanisms in the condensate. Because we did not have the resources to test those more interesting cases and because the case that we did try was not particularly interesting, this set was omitted.

Chapter 4. Analytical Methods

Analytical methods were in development alongside the development of the simulations and data collection. All methods explored or considered are outlined here. In our first method, we looked at the movement of vortices over time for characteristic structures and as an implication of fluid flow. In our second method, we looked at vorticity in the condensate for evidence of potential clustering of vortices that may indicate characteristic structures. In our third method, we applied moving averages to the first two methods in an attempt to reduce noise and find characteristic structures easier. In our fourth method, we try to find evidence of characteristic structures in the velocities of the condensate by analyzing the gradient of the phase of the wavefunction.

4.1 Method 1 – Observing Density Over Time

Density of the condensate is calculated directly from the squared modulus of the wavefunction. In the density of the condensate, small areas of low density indicate the presence of a vortex. As mentioned in Chapter 1 for a 2D BEC in a rotating frame, the quantum phase profile and thus the fluid flow of the entire condensate is approximately analytically implied by the location of vortices. For this reason, we hypothesize that looking for patterns of motion or spatial distribution of the vortices, potential indicators of the development of characteristic structures, might be possible to observe experimentally in the density images of the condensate alone. For this method, we create a video of the density as it changes in time and look for patterns in motion or spatial distribution. As an example, we hypothesized that large rotational patterns might be identifiable by radial motion of vortices. Ultimately, the method is qualitative, making it difficult to differentiate observations that are similar. A quantitative analytical approach would be useful for that type of differentiation.

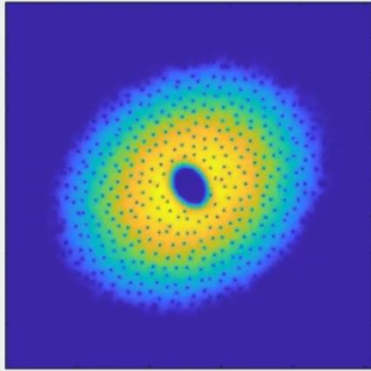


Figure 4.1: A single frame of the video created to observe density over time for set 1, experiment 1 where yellow is high density and blue is low density.

4.2 Method 2 – Observing Vorticity Over Time

In BECs, the velocity at any point is proportional to the phase gradient at that location. Using the velocity field $\vec{v}(x, y)$, a curl of the velocity field, or the vorticity $\omega = \vec{\nabla} \times \vec{v}$, can be calculated. We found this method was successful in the lab frame to help identify both groupings of vortices and the polarity of those groups. An example is shown below.

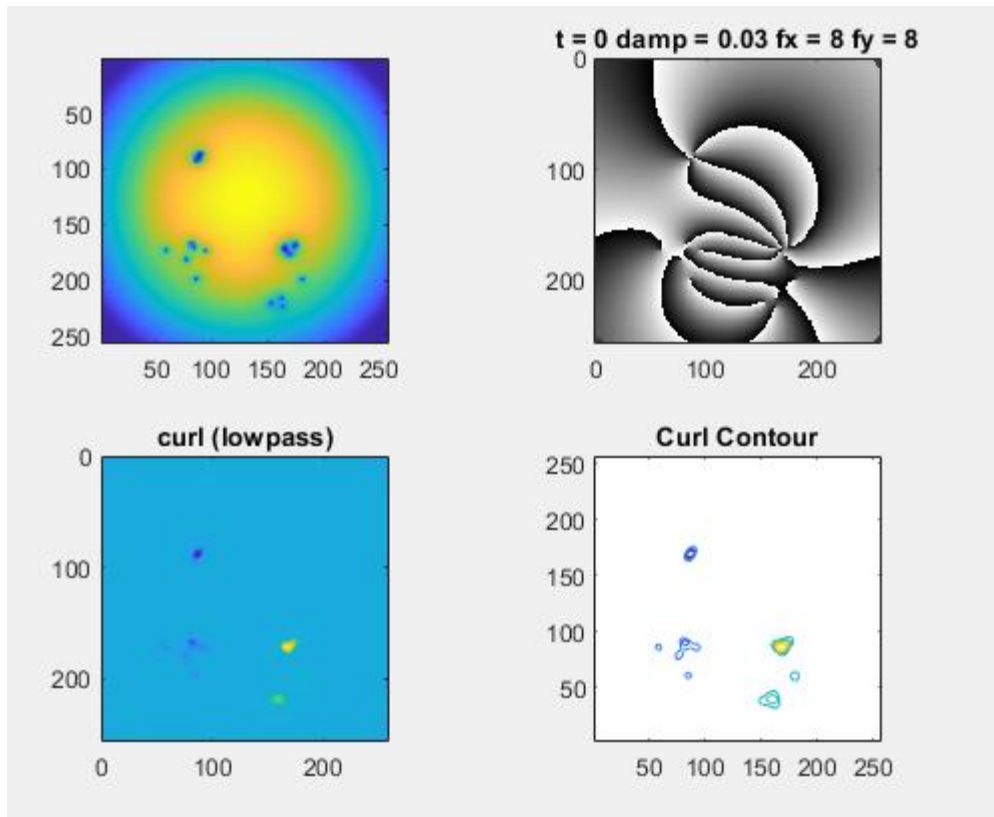


Figure 4.2: An image of our proof-of-concept for using curl of the velocity field to find grouping of vortices. In the top left, the density of the condensate is shown where yellow is high density and blue is low density. In the top right, the phase of the condensate is shown where black is zero phase and white is 2π phase. In the bottom left, the vorticity plot shows grouping and polarity where blue is low vorticity and yellow is high vorticity. In the bottom right, curl is shown again but with levels of contours to compare the ability to show the perceived amount of grouping of the vortices where yellow is higher vorticity and blue is lower vorticity.

4.2.1 Vorticity Analysis Applied to our Data

After the lab frame proof-of-concept seemed to show grouping and polarity of vorticity, we calculated the vorticity of the wavefunctions in our data sets. We found that if any large structure of vorticity does exist in our data that the signal of that large structure is too small

compared to the noise of the vorticity of individual vortices. Several attempts were made at filtering the vortex induced noise out, but a notable signal was not observed in our study. This analysis did not yield results different than observing density changes in time, the density calculations not requiring the extra step in calculation of the curl of the gradient of the phase.

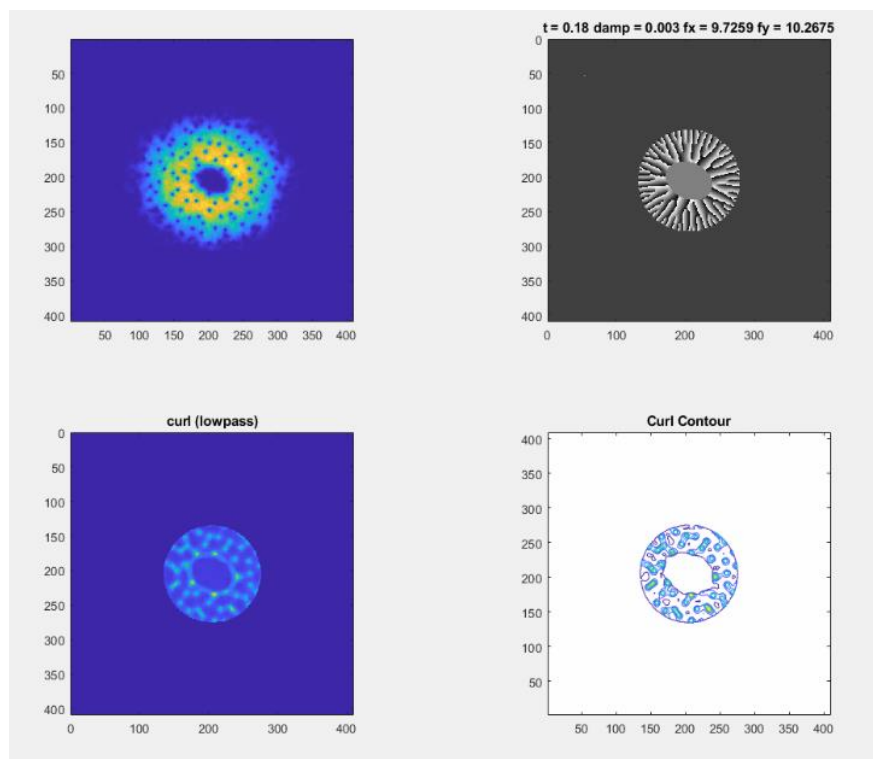


Figure 4.3: An image showing the same vorticity algorithms we applied in Figure 4.2.1, but now applied to our data. In the top left, density of the condensate is shown where yellow is high density and blue is low density. In the top right, the phase is shown where black is zero phase and white is 2π phase. In the bottom left, the vorticity is shown where yellow is high vorticity and blue is low vorticity with one of the many attempted filters. In this case, three filters have been applied: one filter setting the vorticity of the condensate near the eccentric laser to zero, one filter removing vorticity of high spatial frequency, and one filter that replaces each pixel with the median value of the pixels around it. The median filter is what causes the vorticity of the vortices to appear spatially linked to each other by straight lines. Finally, on the bottom right, a contour of the vorticity is shown where yellow is high vorticity and blue is low vorticity.

4.3 Method 3 – Moving Averages

In this method we attempted to reduce the noise in the data by summing a set number of equally spaced chronological images of the density together and dividing by the set number of images. A moving average is created by making a movie that, in subsequent movie frames, recalculates the average by including a new density image and removing the earliest density image. Just like in other methods to this point, the motion of the vortices is really all that is observed by eye. This method can help find patterns of the motion as it gives each of the vortices a “tail” that shows its previous path. In these paths it is possible to see looping motions of the vortices indicating some rotational flow. This method is helpful, but it is a small extension of the density observation and has most of the same limitations.

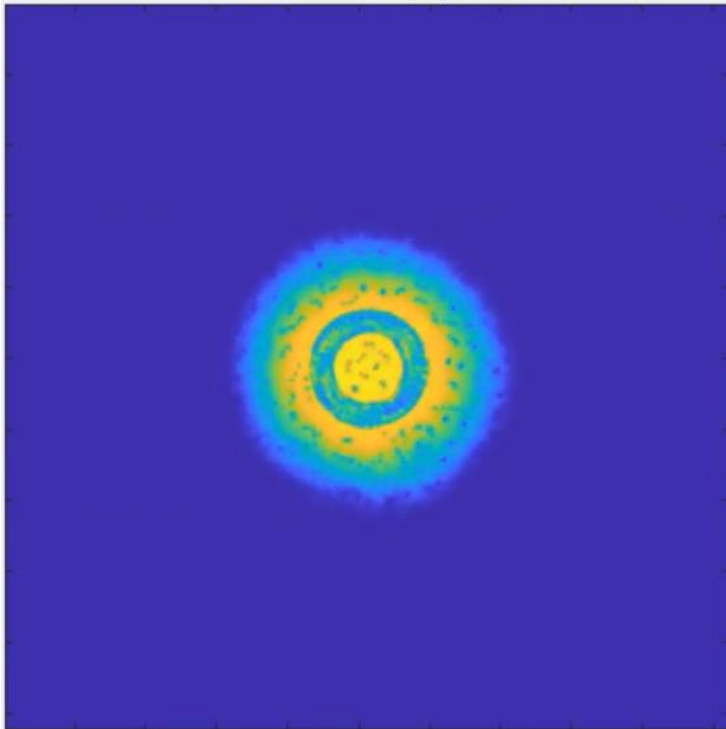


Figure 4.4: An image showing the moving average of the density of set 12, experiment 1. In this example, the moving average helps show the curving trails of vortices in looping motions.

4.4 Method 4 – Speed Maps with Streamlines

Using the phase gradient of the wavefunction with the rotating frame subtracted, a map of speed can be calculated for the condensate. On its own, the speed map was not very interesting as it was dominated by the vortices much like the density or curl maps. However, when streamlines from the same phase gradient with the rotating frame speed profile subtracted are laid over the top of the speed map you can get the visual information of speed of the condensate and the direction of the flow in that location. This seemed to be a very powerful method for finding flow patterns in the condensate.

Using this analytical method, we were able to visually confirm “jet-like” behavior in the “Speckled Annulus” experiment from set 12, experiment 1. Moreover, we had hypothesized that observing movement of the vortices would lead to finding flow patterns in the condensate. We observed rotational motion of the vortices in the density analysis method of the same experiment. This method shows circular flow patterns exactly where we expected them on the edge of the rotating annular laser. The main limitation of this method is that it is qualitative. The other limitation is that the streamlines can be deceiving in areas with very low speeds. Finally, rotation against the rotating frame is possible when subtracting the rotating frame, but this flow in the laboratory frame without a vortex enclosed is forbidden. Circulation is not possible without a vortex according to the Onsager-Feynman quantization condition [1]. A streamline map without rotating frame subtraction is strongly dominated by the rotating frame.

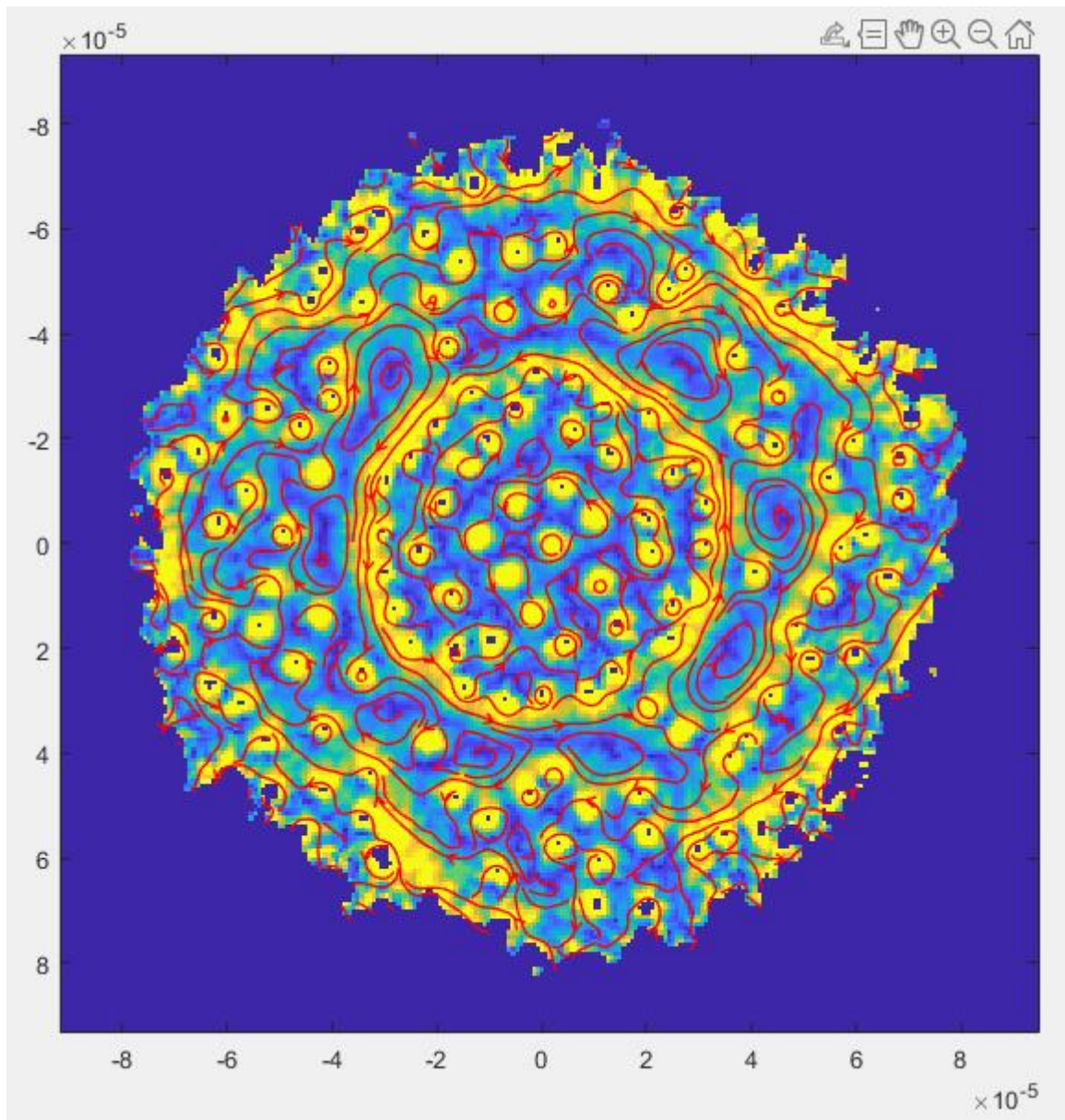


Figure 4.5: A speed map with streamlines showing speed of fluid flow and direction. This analysis was able to show the formation of jet-like behavior and the eddy behavior of the fluid along the outside of that jet. The x -axis displays x positions in meters and the y -axis displays the y -positions in meters (carefully note the 10^{-5} in the corners that indicate that positions in line with the 4 are at position 40 microns, for example).

4.5 Methods not Implemented

This section describes methods not implemented in our study. Those include tracer particles, inspired by the tracer particles of *A Laboratory Model of Saturn's North Polar Hexagon* [3] and energy spectrum plots [5].

4.5.1 Tracer Particles

In *A Laboratory Model for Saturn's North Polar Hexagon* [3], tracer particles are used to show the structural flow and vortices in the bucket. We considered this analytical method for our study as well. The main difficulty is that it will probably not work well with previous data that is often saved thousands of time-steps apart. The trajectory of these particles would likely have to be calculated in real time with the time evolution of the simulation. Future work on this could be fruitful.

4.5.2 Energy Spectrum Plots

It is common in the study of turbulence to look at the energy of the fluid as a function of characteristic length. Some work was done on this, but it was inconclusive. Future work on this analytical method for 2D BECs in a rotating frame could be helpful.

Chapter 5. Conclusion

As a pioneering endeavor into this parameter space for simulating experiments of 2D BECs in a rotating frame with differential rotation, there are several aspects of this work that stand as important contributions to field of BEC physics. Namely, we created a simplified MATLAB framework for quickly simulating many parameter settings on a high-powered computing node with parallel computing via graphical processing units. Then, we found a qualitative data manipulation method that is effective for finding fluid flow structures in a 2D rotating BEC. With this qualitative data manipulation method, we found evidence for counter-rotating eddies in a rotating frame as we had hypothesized. This solidifies our most impactful contribution to the field: evidence supporting the relationship between differential rotation and the observed counter-rotating eddies we hypothesized that would result from that differential rotation.

For future work, there is a lot of room for growth in this small corner of the quantum turbulence field. Towards the end of the study, we started to dive into the possibilities of more complicated laser shapes. Some laser manipulation that could be interesting includes looking at the effect of the annulus on the number and behavior of vortices trapped inside the annulus and on the flow just outside of the annulus. Specifically, in the “Speckled Annulus” experiment of set 12 experiment 1 it would be interesting to see if there is an experimental parameter set that can cause the jet to have more pronounced non-circular instability. In set 4, we observed the importance of the outer bounds of the trap, but in what seems to be our most successful experiments, the annular experiments, there is no treatment of the outer edge of the trap. At the outer range for those experiments the condensate gets very thin and behaves somewhat erratically. There are several options that could be interesting like an abrupt smooth circular boundary or an abrupt rough circular boundary that rotates with the annulus or against it. We hypothesize that the rotation against the rotation of the annulus could create more turbulence like that in set 4. In the final two sets, we saw evidence of characteristic structures. Specifically, we observed significant areas of the condensate that had no vortices. In the speed map analysis with streamlines, we found the streamlines in those areas to be consistent with the hypothesis that it

would be possible to form counter-rotating eddies from differential rotation in the rotating frame. It would be worthwhile to make those structures larger, more stable, and find which parameters can be tuned to find different modes. One thing that went largely unstudied here was the role of the geometry of the bottom of the trap on the system. It is suggested in *A Laboratory Model of Saturn's Northern Polar Hexagon* [3] that a beta effect simulated from a linearly angled trap floor could affect stability of characteristic structures. Any trap floor geometry that varies from the parabolic one explored here could bring useful insight. Finally, quantifying the progression of turbulence in this system remained a challenge for us throughout this study. Future work on this problem may be best suited to look at solutions that utilize vortex identifying algorithms.

Appendix A: Moving MATLAB Calculations to the Graphical Processing Unit

In this appendix, we briefly describe getting started and our experiences with moving MATLAB calculations from a CPU to a GPU.

Using a GPU to calculate FFT's and matrix calculations can provide a significant advantage in speed as the GPU can perform sub-calculations in parallel. In our simulations, an FFT time-evolution method is employed and comprises most of the computational resources of our calculations. A significant reduction in runtime is observed with the GPU method.

With access to the “Parallel Computing Toolbox” on MATLAB the FFT function, `fft()`, supports using the GPU as long as the data is stored in the GPU as a GPU Array. The easiest way to make sure that data is in the GPU is to move all variables in the workspace to the GPU before calculation. In our code, we have a script that does this before beginning the simulation. This script uses the function `gpuarray()` to move the variables in the following way:

$$A_gpu = gpuarray(A_cpu); , \tag{A.1}$$

where `A_gpu` is the array in the GPU and `A_cpu` is the array in the CPU.

With the Parallel Computing Toolbox, this may be the only change required to begin utilizing the GPU for MATLAB calculations; however, there are some other things to consider. For example, let's say a new factor needs to be introduced to a matrix to scale it. If this scalar is introduced after the workspace variables are converted to GPU arrays, and the matrix is then scaled, the data may be moved to a CPU array and the FFT calculated on the CPU. Another challenge that could arise is the compatibility of certain functions. We found that the `imrotate()` function works quite differently on the GPU than on the CPU. On the GPU, the function only takes certain types of data and uses a different interpolation method. Thus, the

GPU version of `imrotate()` is expected to give different results than the CPU version. This difference can be found in the MATLAB help center page of the function under “Extended Capabilities,” then under “GPU Arrays.” For other functions, it is possible to find their differences on GPU in the same location. A full list of GPU-supported functions can be found on MATLAB’s functions page in the help center via filtering by the term “GPU Arrays,” but again, it would be wise to double check that it works on the GPU as expected. We found for example, despite the fact that `imrotate()` is technically supported on GPU, rotating with `interp2()` was easier, faster, and more accurate. Finally, there was a consideration of using single precision variables because GPU calculations are known to be much faster with single precision variables. Unfortunately, for our purposes, we found that this was not enough precision to provide accurate results.

Appendix B: Moving Calculations to The University of Arizona High-Powered Computing Cluster

When computer resources are limited on a researcher's private machine, it may be useful to turn to the use of high-powered computing. The University of Arizona (UA) High-Powered Computing (HPC) cluster gives network access to a system of computers which can store data, run calculations, and output new data. Although a single node is likely more powerful than consumer-level computers, the true advantage comes from being able to run many nodes in parallel. During our study, we ran up to 9 simulations simultaneously on the HPC. This greatly accelerates the process of testing new parameters.

Due to the reliability, flexibility, cost effectiveness, and capability of Linux, servers are typically run with a Linux operating system. Since an HPC cluster is a network of computing nodes it is typical for them to be managed with Linux, a less popular language for researchers. Although only a small amount of Linux is typically needed to interact with the terminals, we had the convenience of a MATLAB Graphics User Interface (GUI) through the Open OnDemand website, and we found that this was sufficient for our needs and time constraints. For that reason and for the potential gain of future University of Arizona affiliates and researchers with similar needs, we briefly describe using that method of interacting with the HPC terminals.

B.1 Starting MATLAB on The University of Arizona's HPC Cluster

- 1) Go to <https://ood.hpc.arizona.edu/>
- 2) Login using your credentials.
- 3) Click on the MATLAB GUI icon.

OPEN

OnDemand

OnDemand provides an integrated, single access point for all of your HPC resources.

Pinned Apps A featured subset of [all available apps](#)

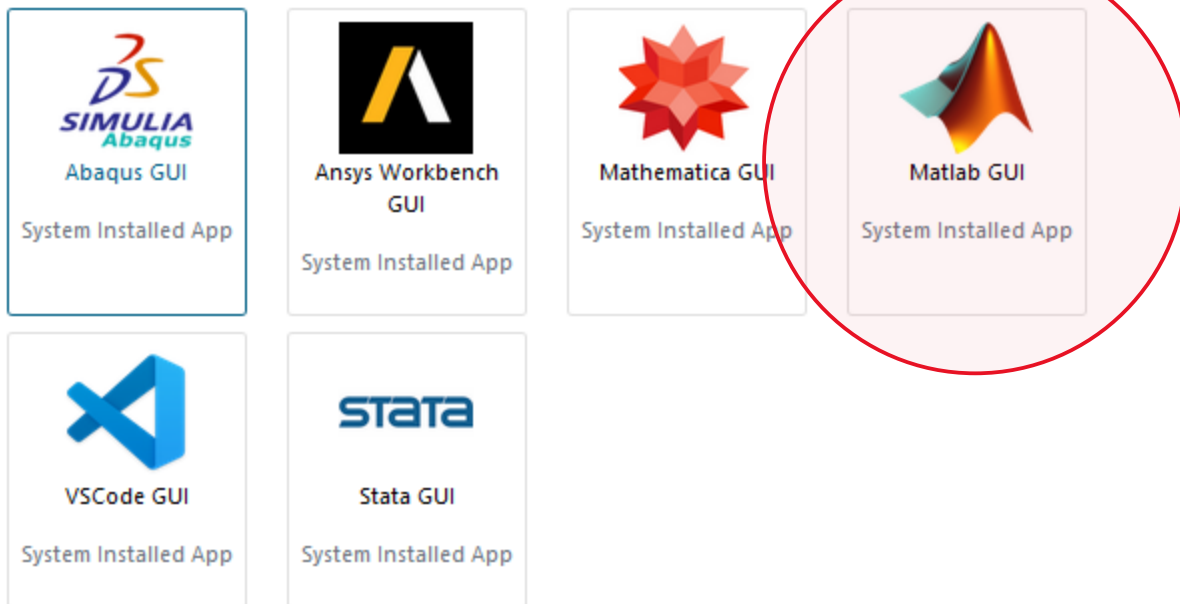


Figure C.1: After logging into the OnDemand website, this is where it is possible to select MATLAB to start a simulation run.

- 4) Choose the number of computational hours desired and identify the PI Group. The other values can remain the same or change based on the needs of the calculation. For this example, we've chosen 3 hours and identified bbanders as the PI Group.

Matlab GUI

This app will launch the [Matlab GUI](#) on a [UAz cluster](#). You will be able to interact with the Matlab GUI through a [Turbo VNC](#) based session.

Cluster

Puma Cluster

I would like to receive an email when the session starts

Matlab GUI version

Default

This defines the version of the application you want to use

Run Time

3

Enter maximum number of wall clock hours the job is allowed to run.

Core count on a single node

2

Enter the number of cores on a single node that the job is allowed to use.

Memory per core

4

Enter the number of Gigabytes of RAM needed per core.

GPUs required

1

Enter number of gpus needed per node, if any.

PI Group

bpanders

Enter an HPC PI group to be charged for time used.

Queue

Standard

Please select a queue from the drop-down above; we **STRONGLY** recommend **AGAINST** using **windfall** here.

Launch

* The Matlab GUI session data for this session can be accessed under the data root directory.

Figure C.2: The GUI that assists the setup of an interactive desktop application instance of MATLAB on the OnDemand website.

- 5) Wait for the queue. This queue took about 5 minutes or less, but some in the past have taken several hours.

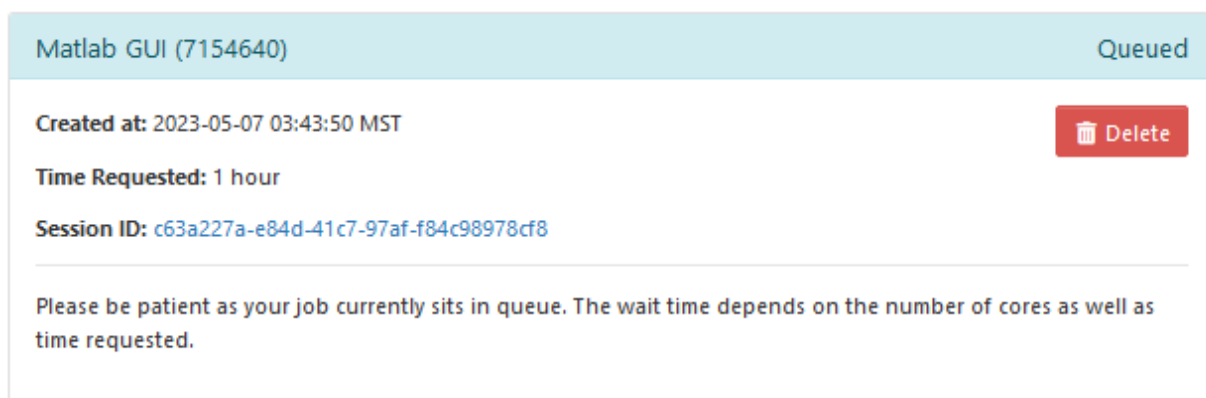


Figure C.3: The GUI showing the MATLAB instance is queued, but not available yet.

- 6) Launch the MATLAB GUI by clicking on the appropriate button.

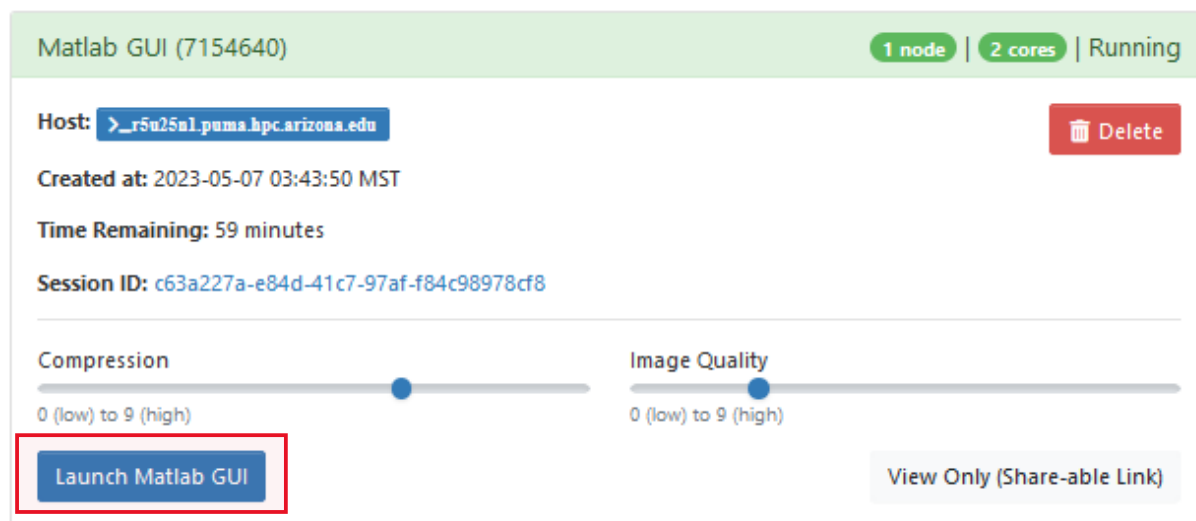


Figure C.4: The GUI in the OnDemand website when the MATLAB interactive desktop instance is ready to launch.

B.2 Downloading/Uploading from/to the HPC

- 1) Go to <https://ood.hpc.arizona.edu/>
- 2) Login using your credentials.
- 3) Navigate to Files and then find your folder.
- 4) Upload or download documents here for use on the HPC.

B.3 Final note on the HPC

On a personal computer the location of files and the file paths for MATLAB may seem a little more intuitive. The biggest change on the HPC is making sure to address the full folder file when loading or writing saves of the data and affirming that all relevant files are on the path for MATLAB.

Appendix C: Using Our Code

In the interest of advancing the research on this topic, this appendix aims to give context to the results presented in the study so that they can be reproduced or tested with new parameters by other researchers. Here we give a brief description of the algorithm then discuss some specific intricacies of using our code.

C.1 General Algorithm

Our basic algorithm consists of the following steps.

- 1) Assign settings and load necessary files.
- 2) Setup coordinate-space and momentum- (or wavenumber-) space grids.
- 3) Convert workspace variables to GPU arrays.
- 4) Run simulation “stages” loop.
 - a. Assign parameters for the stage number, then increase stage number.

- b. Create vectors for dynamic variables: time-steps, damping, laser position, and laser intensity.
- c. Run time evolution loop.
 - i. Initialize variables for time-evolution loop.
 - ii. Calculate dynamic magnetic and optical potentials.
 - iii. Assign dynamic time-step damping parameters.
 - iv. Calculate rotating split-step time evolution.
 - v. Save files at certain checkpoints.
 - vi. Initialize time and iteration number for next stage.

C.2 Stages

Stages in this simulation are basically steps in the process of running the simulation. Most simulations that we ran had two stages. In the first stage, we start with a Thomas-Fermi approximation for a non-rotating ground state BEC in a harmonic trap and evolve the state in time until a ground state in the rotating frame is found with the parameters set. In the second stage, the ground state is perturbed by dynamically changing the optical and magnetic potentials.

Stages can be used to turn on the laser, rotate the laser, translate the laser, turn off the laser, create eccentricity in the magnetic trap, rotate the eccentric trap, and change time-step and damping settings. For our uses, we would usually find the ground state, then turn on the laser, create eccentricity in the trap, and rotate the laser and trap simultaneously. All this can be done with just two stages because of the vectorization of ramping dynamic variables. Some of the variables can ramp up and max out, so that a separate stage is not necessary for constant parameters that have maxed out like laser intensity and eccentricity for example.

C.3 Stages File

The stages file is the main algorithm for the simulation. Few changes to this file should be necessary. The following are what might need to change:

- 1) Settings file script
 - a. This will need to be changed for every simulation with new parameters.
- 2) `new`, `findstart`, `knownstart`, `forceStageIncrease`, and the filename of the known start
 - a. This will be needed if you want to restart the simulation from a known file otherwise the simulation will start from the last save point. They all function as logical binaries with 1 being on and 0 being off.
 - b. `forceStageIncrease` might need to be set to 1 if you happen to start from the very last iteration of the previous stage. Otherwise, leave this at 0.
- 3) Run number, `runNum`
 - a. This can be changed to tag a different number to the saved files. This might be useful if you want to run the same experiment without changing the experiment name. This might be useful to run the same experiment with different save points.
- 4) GPU device, `gpuDevice()`
 - a. Multiple GPUs a single machine may be available, and assigning which GPU was running which simulation can increase efficiency. This is necessary for using the HPC with one GPU node.

C.4 Settings File

The settings file is the most important code segment for setting up a simulation. The stages file mostly just needs to have the settings file in it and know where to start. The settings file has all of the parameters for the code. Due to the evolution of the project, settings files may be setup slightly differently. Here we will describe the latest version, but earlier iterations are similar. If an old settings file is incompatible with the current `Stages`, `time_evolution`, or

similar algorithms, we recommend transcribing those parameters on to the new version of the settings file.

C.5 Contents of the Settings File

- 1) `BEC_constants` script file
 - a. Although this file was rarely changed in our study, it would be the place to change the frequency of the detuned laser and the mass of the atoms used in the experiment.
- 2) `choose Vector`
 - a. This is a convenient way to quickly change differential rotation and damping for comparative studies. The first input chooses the damping multiplier from the `dampM` vector, and the second input chooses the differential rotation multiplier from the `diffM` vector. Leaving the `choose` vector at `[1 1]` is recommended for single experiment use.
- 3) High-level Laser Settings
 - a. There is an option to load in a MATLAB file with a laser shape calculated from a separate script.
 - b. The rotation rate of the laser shape
 - i. For historical reasons this is named `w_conv_laser` to differentiate from a different type of laser rotation.
 - c. An option to change the algorithm for the laser calculation with a script, `I_t_string`. The script is read into the time evolution routine as a string so that changes in the laser algorithm do not require rewriting the entire time evolution routine.
 - d. A string that calculates the max power of the laser, `P_max_string`.
- 4) Potential Definition

- a. Calls functions that define the potential energy and interaction energy. Similar to the High-level Laser Settings, this allows modification without rewriting the main routine of the code.
- 5) Trap settings
- a. Range is the full width of the spatial domain in the x -direction and y -direction.
 - b. The desired spatial resolution will not be the actual resolution because there is a routine to guarantee that the spatial domain is equal to a base 2 exponential for faster calculations. The resolution will always be smaller than desired.
 - c. R is a guess at the Thomas-Fermi Radius; however, this value is not used in any calculations anymore.
 - d. N is the number of atoms.
 - e. $LAMBDA$ is a fudge factor for vortex insertion algorithms.
 - f. The healing length correction is a second fudge factor for vortex insertion algorithms.
 - g. Resonant frequencies of the magnetic trap.
- 6) Settings related to the spinning of the eccentric magnetic trap
- a. Eccentricity, geometric mean, scalar, initial trap frequencies, etc.
 - b. Frequency of trap rotation, ω_c
 - c. Time in seconds to ramp up the eccentricity of the trap, ecc_ramp
- 7) Calculations from settings used later.
- a. Interaction Coefficient script
 - i. This script calculates chemical potential, Thomas-Fermi Radius, interaction coefficient, healing length, and reduced interaction coefficient in the 2D limit from the given trap frequencies, scattering length, and mass, and number of atoms.
 - b. Calculation of the size of the spatial domain in pixels, referenced in code by the variable name “ $r1$ ” which indicates resolution of the first kind (although a second kind was never needed or established), to ensure that the number of pixels in the array is equal to an exponential of base 2 for efficient calculations.

- c. Characteristic oscillation time of the trap, not used in any calculations.
- 8) Laser Motion Settings
- a. Settings for translating the laser
 - b. Eccentricity and dimensional widths of the laser
 - c. Energy and maximum power of the laser
 - d. Frequency of rotation of the laser
 - e. Ramp up time of the laser
 - f. Time to observe the condensate after translating the laser (this will not work unless it is put in the `time_Stages` settings)
- 9) Gaussian manipulation settings
- a. This is no longer used, but left for testing, if necessary.
- 10) Data saving settings
- a. `filename_0` is a convenient way to name the outputs of imaging algorithms. Most imaging was not done on the HPC and best practice on the HPC is to specify the folder of the save which has not been done here.
 - b. `skip_images`, `pot_lim`, `phase_lim`, and `phase_grad_density` have all been antiquated. These types of imaging settings are better suited to imaging scripts.
 - c. `skip_saves` allows a large reduction in data size by only saving certain iterations of the `time_evolution` routine. The iterations saved are multiples of the `skip_saves` value.
 - d. `experimentName` is the name of the experiment.
 - e. `folderName` is the name of the folder. This is very important for saving in the HPC.
 - f. There is a string that writes all relevant information into a predictable file name for saving. This system allows the Stages file to start calculation at the last saved iteration.
- 11) Settings for the Stages (# is the stage number, starting at 1)
- a. Number of stages and the stage to start at

- b. Base time-step, `dt_0_#`
- c. Vector of damping values, `damp_V_#`
- d. Vector of time durations, `tmax_V_#`
- e. Time-step vector, `dt_V_#`
- f. Starting time-step, `dt_#`
- g. Starting damping, `damp_#`
- h. Binary to spin eccentric trap, `spin_condensate_#`
- i. Binary to ramp up eccentricity of condensate, `ramp_ecc_#`
- j. Initial max power of laser, `P_t0_#`
- k. Ramp up laser power, `ramp_up_#`
- l. Ramp down laser power, `ramp_down_#`
- m. Translate the laser, `translate_laser_#`
- n. Convolve one laser shape with another shape, `conv_laser_#`
- o. Rotate the entire laser shape, `rotate_conv_#`
- p. Frequency of reference frame, `W_rf_#`
- q. Frequency of laser shape rotation, `W_l_#`
- r. Adding a variable that changes with stage number follows this algorithm. Add it to the list here with the “#” format and then add it to the `time_Stages` file in the Routines and Constants folder in the format of the other variables listed. This will break compatibility with other settings files, but it can be fixed by adding the new variable to the old settings file.

12) Calculation of run time

This is no longer accurate because of updates to routines and movement of calculations to the HPC; however, there are hard-coded fudge factors in the estimated run time calculation that can be easily changed to accommodate the current system.

References

- [1] Pethick, C. J. and Smith, H. Bose–Einstein Condensation in Dilute Gases. Cambridge: Cambridge University Press, 2008. <https://doi.org/10.1017/CBO9780511802850>
- [2] Galperin, Boris and Read, Peter L. (2019). Zonal Jets : Phenomenology, Genesis, and Physics. Cambridge University Press. <https://doi.org/10.1017/9781107358225>
- [3] Barbosa Aguiar, Ana C., Read, Peter L., Wordsworth, Robin. D., Salter, Tara., and Yamazaki, Y. Hiro (2010). A Laboratory Model of Saturn’s North Polar Hexagon. *Icarus* (New York, N.Y. 1962), 206(2), 755–763. <https://doi.org/10.1016/j.icarus.2009.10.022>
- [4] Anderson, Brian P. (2010). Resource Article: Experiments with Vortices in Superfluid Atomic Gases. *Journal of Low Temperature Physics*, 161(5-6), 574–602. <https://doi.org/10.1007/s10909-010-0224-1>
- [5] Bradley, Ashton S. and Anderson, Brian P. (2012). Energy Spectra of Vortex Distributions in Two-Dimensional Quantum Turbulence. *Physical Review X*, 2(4), 041001. <https://doi.org/10.1103/PhysRevX.2.041001>
- [6] L'vov, Victor S. (1998). Universality of Turbulence. *Nature* (London), 396(6711), 519–521. <https://doi.org/10.1038/24998>
- [7] NASA Juno Findings - Jupiter’s Jet-Streams Are Unearthly. NASA. Retrieved August 17, 2023, from <https://www.nasa.gov/feature/jpl/nasa-juno-findings-jupiter-s-jet-streams-are-unearthly>
- [8] Photojournal. Jet Propulsion Laboratory. (2018, March 7). Retrieved August 17, 2023, from <https://photojournal.jpl.nasa.gov/catalog/PIA20513>
- [9] Feit, M.D, Fleck, J.A, and Steiger, A. (1982). Solution of the Schrödinger Equation by a Spectral Method. *Journal of Computational Physics*, 47(3), 412–433. [https://doi.org/10.1016/0021-9991\(82\)90091-2](https://doi.org/10.1016/0021-9991(82)90091-2)

- [10] Hodby, E., Hechenblaikner, G., Hopkins, S. A., Maragò, O. M., and Foot, C. J. (2002). Vortex Nucleation in Bose-Einstein Condensates in an Oblate, Purely Magnetic Potential. *Physical Review Letters*, 88(1), 010405. <https://doi.org/10.1103/PhysRevLett.88.010405>
- [11] Wilson, K E, Samson, E. C., Newman, Z. L., Neely, T. W., and Anderson, B. P. (2013). Experimental Methods for Generating Two-Dimensional Quantum Turbulence in Bose-Einstein Condensates. *Annual Review of Cold Atoms and Molecules*, V. 1, Ch. 7, 261. World Scientific, Singapore. https://doi.org/10.1142/9789814440400_0007
- [12] White, Angela C., Barenghi, Carlo F., and Proukakis, Nick P. (2012). Creation and Characterization of Vortex Clusters in Atomic Bose-Einstein Vondensates. *Physical Review A*, 86(1), 013635. <https://doi.org/10.1103/PhysRevA.86.013635>
- [13] Choi, S., Morgan, S. A., and Burnett, K. (1998). Phenomenological Damping in Trapped Atomic Bose-Einstein Condensates. *Physical Review A*, 57(5), 4057–4060. <https://doi.org/10.1103/PhysRevA.57.4057>